



Agricultural Science and Resource
Management in the Tropics and Subtropics
(ARTS)



Institut für Nutzpflanzenwissenschaften und Ressourcenschutz (INRES)
Crop Science and Plant Breeding
Department of Crop Science and Resource Conservation



Zentrum für Fernerkundung der Landoberfläche (ZFL)
Centre for Remote Sensing of Land Surfaces

GROUND AND SATELLITE BASED DETECTION OF RANGELAND MANAGEMENT IN PER HUMID GRASSLANDS OF ARGENTINA

Thesis

in partial fulfilment of
the requirements for the
academic degree of

Master of Science

of the

Faculty of Agriculture

Rheinische Friedrich-Wilhelms-Universität zu Bonn

Submitted on January 2007

by

Ditmar Bernardo Kurtz

Argentina

Table of contents

Table of contents.....	I
Abstract.....	III
Abbreviations.....	IV
List of figures.....	VI
List of tables.....	VIII
I. Chapter 1. Introduction	1
a. The problem	3
b. Remote sensing based biomass estimation.....	6
c. Land cover classification	7
d. Hypothesis and objectives.....	9
II. Chapter 2. Material and methods.....	10
a. Study area.....	10
b. Imagery	12
1. Imagery and image pre-processing	12
2. Imagery normalization	13
3. Vegetation indices	14
4. Biomass estimation	15
5. Land cover classification.....	16
6. Stocking rate calculation.....	19
c. Ground truth data collection	19
1. Experimental design	19
2. Laboratory evaluations	20
3. Validation of biomass estimation	21
4. Landscape survey	22
III. Chapter 3. Results and discussion.....	23
a. Normalized imagery	23
b. Site characterization and site assessments	24
c. Assessments working with historical data	28
d. Relationship between biomass and vegetation indices	29
1. Historic data.....	30
2. Current data.....	32
3. Validation of biomass estimation	35
4. Spectral characteristics of the two grassland types	37
e. Land cover classifications	38
1. Image selection	38

2. Supervised classification	40
3. Number of bands and the roll of ancillary data	45
4. Accuracy assessments	48
f. Stocking rate calculation	50
IV. Chapter 4. Conclusions	51
References.....	54
Appendices.....	61
<i>Curriculum vitae</i>	100

Abstract

Ranging is the most important single agricultural activity in the department of Empedrado, in the province of Corrientes, Argentina. The present study focuses on three issues (i) the classification of land cover types, (ii) the evaluation of range intensity use and (iii) the estimation of aboveground biomass.

First, a multi-temporal Landsat image analysis, including supervised classification and ancillary data, was used to enable an accurate land cover classification. Second, by plotting historical biomass information and Landsat calculated NDVI, a simple regression model was calculated. Third, with the previous land cover information and statistical, up to date stocking rates were calculated.

By comparing radiometrically normalised and not normalised images it could be demonstrated that imagery normalization was not always necessary, when comparing NDVI values. Regarding biomass estimation, neither a simple nor an averaged point approach provided accurate results. The inverted distance weighted interpolation method showed better biomass estimates in per-humid grasslands. Two maps were achieved for Empedrado, one 26-class land cover map and one 8-class land grazing intensity map. The classification accuracy strongly relied on ancillary GIS based information. The resulting maps showed that intensive grassland use was the most common vegetation on the hills, whereas not intensively used and burned areas were prevailing on the plains.

The calculation stocking rates of grasslands with Landsat images was possible as long as additional statistical data were available.

Abbreviations

ANOVA	analysis of variance
AOI	area of interest
A. U.	animal unit
AVHRR	advanced very high resolution radiometer
BS	bare soil
B1... 7	Landsat band one to band seven
CONAE	Comisión Nacional de Actividades Espaciales
cv	coefficient of variation
DMY	dry matter yield
DWRM	dry weight rank method
FAO	Food and Agriculture Organization
FOO	feed on offer
FUCOSA	Corrientes Animal Health Foundation
GCP	ground control points
GIS	geographic information system
GLCF	Global Land Cover Facility
GPS	global positioning system
Ha	hectare
IDW	inverted distance weight
INDEC	Instituto Nacional de Estadística y Censos
INRES	Institut für Nutzpflanzenwissenschaften und Ressourcenschutz
INTECO	trend and cover index
INTA	Instituto Nacional de Tecnología Agropecuaria
LCCS	land Cover classification system
LGP	length of the growing period
M	mulch
µm	micrometer
MIR	reflectance in the middle infrared portion of the electromagnetic spectrum
MrSID	multi-resolution seamless image database
NDVI	normalized difference vegetation index
NE	north-eastern
NIR	reflectance in the near infrared portion of the electromagnetic spectrum
PIFs	pseudo-invariant features

R	reflectance in red portion of the electromagnetic spectrum
RS	remote sensing
RMS	root mean square error
S	south
SAVI	soil adjusted vegetation index
SDM	standing dead material
SGB	standing green biomass
SRTM	shuttle radar topography mission
TM	thematic mapper
USGS	United States Geological Survey
UTM	universal transverse mercator
W	west
WGS 84	world geodetic system 1984

List of figures

Figure 1. Eco-graph depicting the grazing intensity gradient in the two most important grassland types in Empedrado.....	2
Figure 2. Total livestock share in the Empedrado department.....	3
Figure 3. Cattle population evolution expressed in A. U. Comparison between Corrientes province and Empedrado department.....	5
Figure 4. North-Eastern Argentina - Corrientes province. False colour composite Landsat TM image of Empedrado Department.....	10
Figure 5. Schematic representation of the classification showing the integration of multi-band imagery and ancillary data.....	17
Figure 6. Plot of NDVI values calculated from radiometrically normalised and not radiometrically normalised cloud free images.....	23
Figure 7. Plot of NDVI calculated from a radiometrically normalised image against NDVI values from a not radiometrically normalised image under cloudy conditions.	24
Figure 8. Biomass composition.....	26
Figure 9. Relationship between INTECO and SDM.....	27
Figure 10. Relationship between INTECO and NDVI calculated from historical data sets. A, shows different paddocks, and B shows different seasons.	29
Figure 11. Relationship between total biomass, and NDVI.....	30
Figure 12. Relationship between C. V. of total biomass and C. V. of NDVI.....	31
Figure 13. Plot of the coefficient of variation of NDVI against the C. V. of biomass values in different seasons.....	32
Figure 14. Relationship between NDVI and single point-biomass values.	34
Figure 15. Relationship between NDVI and point-average biomass values.....	34
Figure 16. Relationship between NDVI and interpolated biomass values.....	34
Figure 17. Relationship between SAVI and interpolated biomass values.	35
Figure 18. Estimated biomass calculated from each individual NDVI, plotted against each single measured biomass.....	36
Figure 19. Estimated biomass calculated from individual NDVI, plotted against measured block-averaged biomass.....	36
Figure 20. Estimated biomass calculated from individual NDVI, plotted against interpolated calculated biomass. Regression equation is shown in A and validation concerning each site in B.....	37

Figure 21. Grassland variability indicated by IDW interpolated green biomass values (left). Landsat pixel based interpolation of green biomass (right).	38
Figure 22. Major land cover classes in Empedrado department classified from satellite images.	39
Figure 23. Relationship between occupied area of the five major land cover classes and accumulated precipitation of the previous year.	39
Figure 24. Map showing the integrated land cover classification for Empedrado.	41

List of tables

Table 1. Scenes and registration characteristics of the used images.	12
Table 2. Dry biomass on the hill site expressed as dry matter for the five principal species.	25
Table 3. Dry biomass on the plain site expressed as dry matter for the five principal species.	25
Table 4. Average INTECO and average NDVI calculated from current winter data sets.	27
Table 5. Comparison between BS and M on hills and on plains.	28
Table 6. Integrated land cover classification after combining satellite imagery and ancillary data.	42
Table 7. Land cover-land use intensity classified area.	44
Table 8. Comparison of land cover area classified using 6 or 12 Landsat bands.	46
Table 9. Prevailing soil types in the different areas in Empedrado.	48

I. Introduction

On an area basis, grasslands contributes most to the worlds land surface ([Guo et al., 2000](#)) being mainly devoted to range use. Management of these areas alters drastically its natural characteristics. As a result, biomass quantity, biomass quality, biodiversity and nutrients cycles are strongly influenced. Therefore, is very important to understand feeding patterns, recognize degradation trends and livestock management. An accurate land cover estimation and evaluation can potentially support the appropriate management. Climate is another important factor contributing to modify grasslands since it is a key factor that controls grass growth.

Nowadays, the actual trends and the favourable agricultural situation in the whole world including Argentina, are suggesting an increasing pressure on the environment in all natural and semi-natural areas. In Argentina, grasslands cover most of the agricultural area. The mentioned grasslands are often also referred as rangelands, in the following only the former is used following the criteria used by [Di Gregorio et al.](#) (2005) who understand that rangelands is a kind of land use and not a land cover term. With 140 millions hectares dedicated to cattle production, grasslands correspond to the largest area, whose fraction varies depending on the region. Regions with fertile soils are since long time being devoted to agriculture, whereas shallow or poor soils, located in marginal areas, are mainly devoted to livestock production. The latter is the case in the province of Corrientes, covering a total area of 8.9 million hectares.

Raising cattle is the most important agricultural activity and key of the province's economy. Continuous grazing all year round, in nearly 6.7 million hectares is the most frequent situation. The supply of additional fodder or the utilization of artificial pastures is not frequent. As a result, often low secondary production levels are achieved. On the other side, high levels of primary production are achieved based on C₄ grasses. During the winter time, feed on offer (FOO) decreases, not only in quantity but also and mainly in quality.

Even during summer with low stocking rates, the dry FOO not consumed by livestock remains accumulated on the fields. To remove this leftover material, the most common tool used is fire.

In an early work, [Deregibus](#) (1988) calculated the potential carrying capacity of different grasslands in Argentina. He mentioned that for the Corrientes region this value was 0.9 A. U. ha⁻¹. Stocking rates below that produced areas with leftover material whereas higher stocking rates may result in overgrazed areas. Besides, [Carnevali](#) (1994) calculated the specific stocking rates for the Corrientes province. He concluded that the stocking rate was 0.6 to 0.8 A. U. ha⁻¹. He also warned that the threshold is almost being reached and that excess grazing lead to grassland degradation.

Grasslands are often subjected to different grazing pressure. Intensively grazed grassland is recognized because of very short grasses and often different proportions of bare soil (BS). On the other side, less grazed areas accumulate dry material mixed with green vegetation.

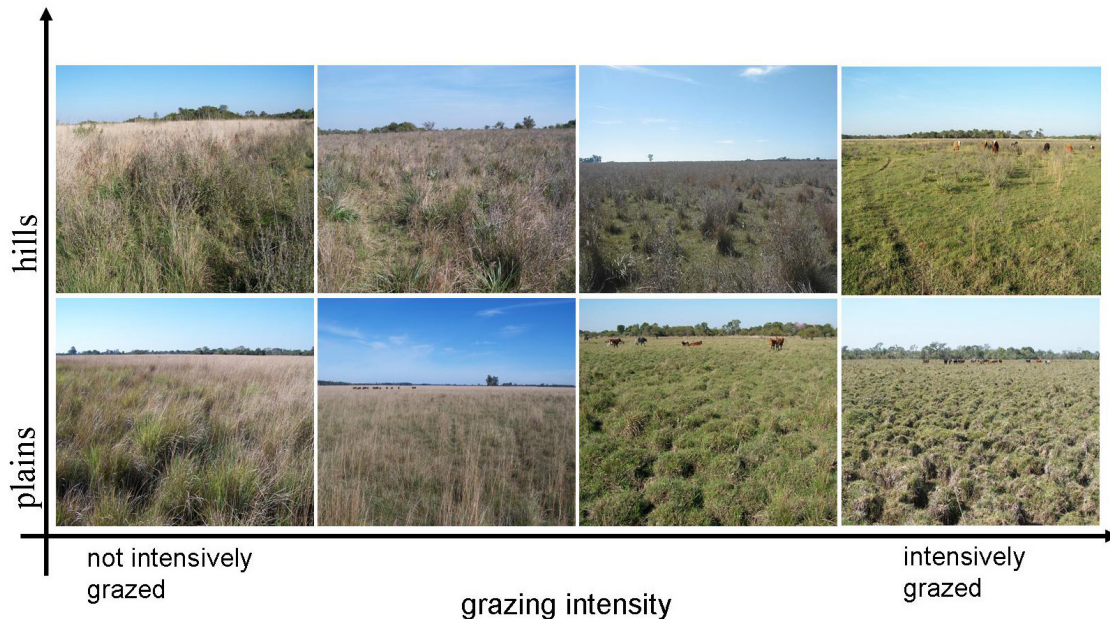


Figure 1. Eco-graph depicting the grazing intensity gradient in the two most important grassland types in Empedrado (located on hills and on plains). Plains shaped by reticular erosion.

On figure 1, a grazing intensity gradient was depicted. Differences in management produced less intensively grazed areas, as shown on the left, to intensively grazed grasslands, as shown on the right. Differences regarding soil cover and soil erosion were also evident between hills and plains. In the latter, a strong “reticular” erosion pattern was normally present.

The two different features mentioned above were also recognizable on the Empedrado department, namely intensively and not intensively grazed (or under-grazed), (fig. 1).

In Empedrado cattle represented the largest fraction of the livestock that continuously graze all year round (fig. 2). A better understanding of the actual rangeland status in larger scale was needed, in order to take objective decisions. Remote sensing and GIS tools, satellite imagery and ground truth data were therefore used in this study.

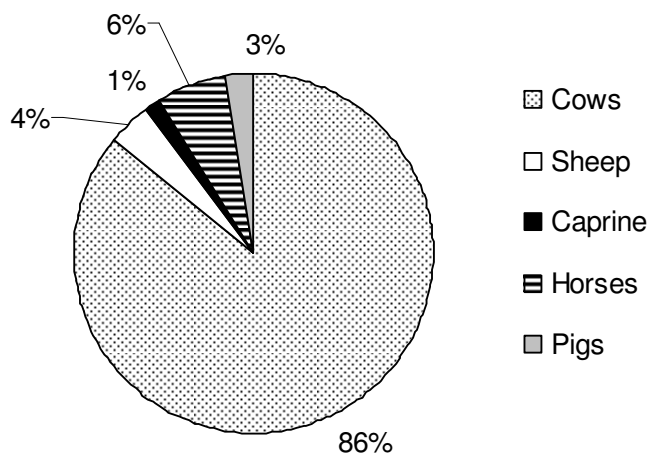


Figure 2. Total livestock share in the Empedrado department. Source: INDEC, national agricultural census 2002.

a. The problem

Land cover estimates indicate that the grassland cover 96691 ha in Empedrado ([INDEC 2002](#)). Precise land cover information and not subjective

estimates is needed in order to achieve sustainable natural resources management. Regarding grasslands utilization an exact knowledge of the following three main factors is required: (i) the exact area to be grazed, (ii) the total amount of grazing animals on that area and (iii) present biomass on the field.

The first factor, area, is sometimes, already known by the rangers since they have accurate cadastral planes. However, only the total farm area is known and normally paddock size is estimated. Additionally, the total area often increases or decreases due to newly incorporated or sold areas. Nowadays, this situation can be overcome with the aid of cheap GPS equipments that are increasingly used. As a result, total farm or paddock areas can easily and accurately be calculated. Besides, there is a remaining issue: land cover classification. Not only total paddock or farm size is needed, but also the area shared by forests, lagoons, swamps and marshes is important, since all these areas have different potential range use compared to pure grassland. Therefore, its quantification is of huge interest when trying to calculate net available grazing area.

The second factor, livestock, is often known quite accurately. Stocking rates should be calculated on a common basis system, since logically different categories have different feeding requirements.

The third factor, biomass, is normally estimated or measured on the field. *In situ* available feed assessment is normally very time consuming and estimates useful only on a paddock level. Different regions, landscapes, paddocks and even areas across them often show strong variations. Regarding this factor, an additional issue is that not all biomass is consumed by cows (weeds or toxic plants for example) because the animals select some plant parts in preference to others and some species rather than others ([Pearson *et al.*, 1997](#)). It means that not all of the present biomass is palatable. Therefore, botanic composition plays an important role in view of determining forage quality.

Traditional studies to assess forage quantity and quality have been conducted for long time in Corrientes ([Bernardis et al., 2005](#)). Biomass measurements are very time consuming. Therefore, fast and objective methods are needed. Remotely sensed data could provide a very objective and continuous source of information for predicting green biomass levels ([Anderson et al., 1993](#), [Edirisinghe et al., 2004](#), [Everitt et al., 1989](#), [Kelly et al., 2003](#)). Deriving significant relationships between ground and satellite data may help to estimate biomass by saving time, resources and operational expenses.

Stocking rate is the land area allocated per livestock unit for a specific time. Total livestock in Empedrado is known quite accurately. Determining the stocking rates is important for grassland management and also to detect degradation trends, since it influences not only superficial soil layer but also inherent grassland properties.

In Corrientes, the trend of cattle population shows an exponential increase in the last five years. On the other side, in Empedrado, cattle population increase was not so spectacular (fig. 3). Different reasons could be attributed to this lower increase and, difficulties in management may not be the triggering cause, but a very important one. Besides that, the stocking rate in Empedrado also increased in the last years.

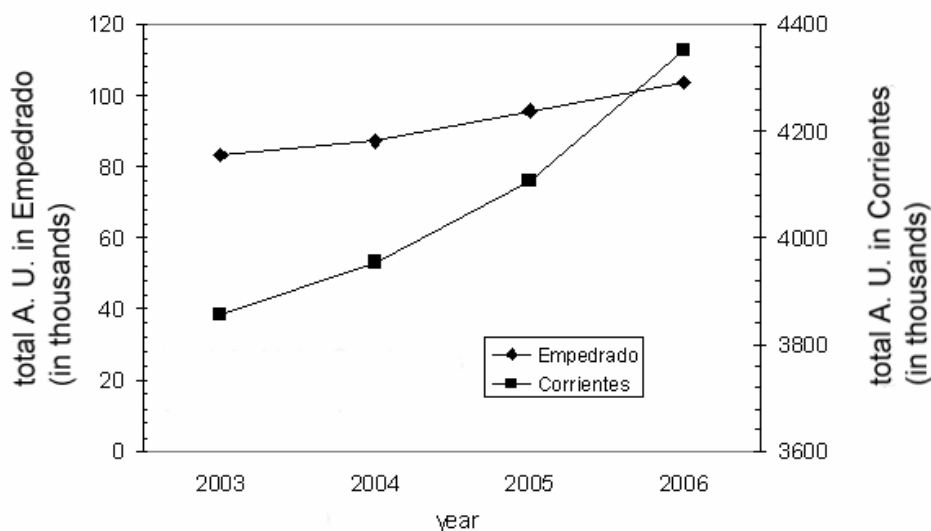


Figure 3. Cattle population evolution expressed in A. U. Comparison between Corrientes province and Empedrado department. Source, FUCOSA, 2006.

Finally, for an accurate stocking rate calculation, not only total animal units but also accurate area should be considered.

b. Remote sensing based biomass estimation

Very advanced remote sensing methods are used to estimate different biophysical parameters of the vegetation, like pasture growth rate ([Hill et al., 2004](#)), pasture quality ([Dymond et al., 2006](#)) and primary production ([Paruelo et al., 2000](#)).

Regarding satellite based biomass estimations, in a review paper [Tucker \(1980\)](#) indicated that the non-destructive spectral method (remotely sensed) of biomass estimation has shown to work well for large area surveys, but tied to the specific cover type. [Tucker et al. \(1985\)](#) also indicated that NDVI produces useful estimates of green leaf-biomass dynamics. But, [Tucker et al. \(1986\)](#) also emphasized that the reflectance data could hardly provide an estimation of the vegetation state, such as leaf area index or biomass.

After that, it has also been reported that NDVI derived from NOAA-AVHRR data provides a sensitive tool for monitoring changes in the vegetation status, for example in Tunisia's grazing lands ([Kennedy 1989](#)). Additionally, it was pointed out that grassland management requires imagery with finer spatial resolution than NOAA-AVHRR possesses (1.1km), due to the spatial heterogeneity on a scale of square meters ([Di Bella et al., 2004](#), [Ikeda et al., 1999](#)). Such kind of vegetation heterogeneity is frequent in Corrientes. Therefore, better perspective was expected by using Landsat images with higher spatial resolution.

The potential estimation of grassland biomass on rangelands with Landsat imagery was already shown in an early study by [Everitt et al. \(1989\)](#). They found a strong relationship between "phytomass" and spectroradiometric canopy reflectance when working with combined NIR and MIR bands. Besides that, [Li Jianlong et al. 1998](#) found that the combination of remote sensing and

ground truth data were useful to estimate grassland yields over large areas, in China.

Working with Landsat imagery [Guo et al.](#) (2000) found that species composition differently affected reflectance. They suggested that biomass estimation would be significantly influenced by the arrangement of grasses and forbs. Also in semiarid rangelands, [Anderson et al.](#) (1993) showed that no significant relationship between vegetation indices and biomass can be expected when using a sample point approach. They found a stronger relationship by spectrally grouping the original dataset (using R, NIR and MIR for a non supervised classification) and obtaining average NDVI values in homogeneous areas. Unfortunately, the estimation was not always significant. They finally obtained better estimation of green biomass when using a simple univariate model by combining biomass and previously arranged NDVI values. They conclude that it is possible to estimate biomass from Landsat TM images but, the degree of association is substantially influenced by the method used to combine the sources of information. Finally, very accurate Landsat TM5 and 7 remote sensed estimates of pasture biomass were achieved in Australia ([Edirisinghe et al., 2004](#), [Kelly et al., 2003](#)). The latter mentioned that NDVI could explain up to 73% of variation in biomass estimates when working in pastures.

c. Land cover classification

To know the area occupied by different land covers helps for a better stocking rate calculation. It is not the same to have high tree coverage or areas with marshes (hardly able to feed cattle) or pure grassland. This is evident because the more trees (or marshes) exist the less grass is available to the livestock. Additionally, mapping land cover types provides key information for the analysis of agricultural activity, carbon accounting and landscape function and diversity ([Hill et al., 2005](#)).

At present, attempts to map land cover classes and especially grasslands

have successfully been made in arid and semi-arid environments when working with RS data ([Evans et al., 2006](#), [Laliberte et al., 2004](#)). On the other hand, in tropical and subtropical regions, fewer attempts to classify land cover have been reported ([Seyler et al., 2002](#)). In all cases, classifications have only considered few and very broad land cover classes, such as forest, water and urban areas. Finally, [Hill et al. \(2005\)](#), who combined optical and radar data, demonstrated that the use of ancillary data allow for a discrimination of more classes, rather than working with a simple image.

It is known that when a larger coverage area is needed, RS plays a central role in resource evaluation, not only at different temporal resolutions but also at different scales.

d. Hypothesis and Objectives

Hypothesis

Satellite based biomass estimations and accurate land cover information support appropriate livestock management. It is an objective tool to identify land degradation on Empedrado's landscapes areas. This work is therefore not focused on a paddock level, but rather on a departmental scale.

Objectives

The development of an objective tool that contributes to more efficient grassland utilization in the NW of Corrientes

The present project was to develop a technique that allows to

1. accurately identify vegetation types within a rural area dominated by agricultural land in the NE of Argentina (land cover classification)
2. separate various grasslands types from the remaining agricultural land and so to distinguish between land use intensity levels (land use classification)
3. estimate biomass on the relationship between satellite imagery and ground truth information
4. estimate the grazing pressure in Empedrado's grasslands, by accurate calculation of the current stocking rates

II. Material and Methods

a. Study area

The study area is the Empedrado Department in North-Western Corrientes, Argentina (fig. 4). The province of Corrientes is located in the North-Eastern of the Republic of Argentina.

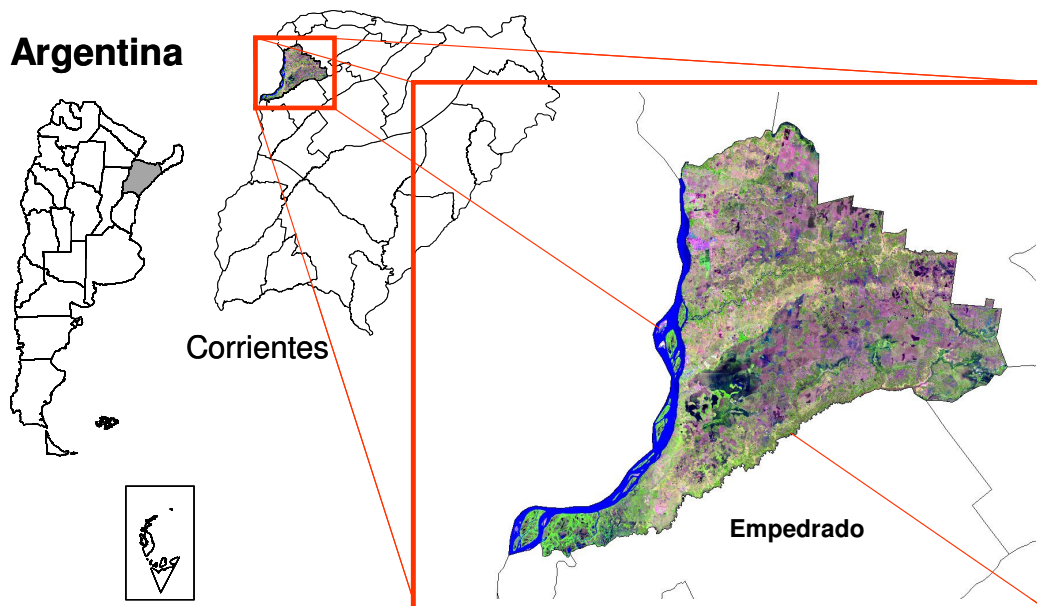


Figure 4. North-Eastern Argentina - Corrientes province. False colour composite Landsat TM image of Empedrado Department.

Empedrado department has a total area of about 191976 ha. It receives between 1200 - 1300 mm of precipitation per year, with 56% falling from October to April. For the noted characteristics we can neither see markedly dry nor markedly wet season. The average annual temperature ranges from 20.7 to 21.5°C, with a mean monthly maximum temperature of 26.5 to 27.5°C in January and a mean monthly minimum of 15.0 to 16.0 in July ([Escobar et al., 1996](#)). The length of the growing period (LGP) is 330 days and was calculated with the FAO developed software Cropwat for windows. As a result, the climate is classified as per-humid. There is no clear dormant season for the vegetation.

Perennial summer grasses dominate in the department, mainly warm-season species (C₄ photosynthetic pathway) growing from spring to autumn. Low winter production and poor herbage quality are major limiting factors in livestock production ([Royo Pallarés et al., 2005](#)).

Empedrado's landscape (as part of the Corrientes province) was shaped by sandy depositions originated in the Paleozoic, belonging to the sedimentary Paraná River basin. Very soft hills constitute the positive element of the relief, which are never more than 10 meters above the associated plains. The soils on the hills are sandy, and parks and savannas are the predominant vegetation forms. Among the hills, plains are located, where a water table normally remains for several months on the soil. On plains, the predominant physiognomies are also savannas, generally including waterlogged or periodically flooded areas.

Dominant species in the hills are *Andropogon lateralis* Nees, *Sorghastrum agrostoides* (Speg.) Hitchc. and *Paspalum notatum* Flügge. In the plains *A. lateralis* and *S. agrostoides* are also found as dominant species, mainly because they grow on the top of mounds shaped by "reticular erosion" (fig. 1). But, when flooding or permanent swampy conditions occur, other short grasses develop. *Axonopus affinis* Chase grow in the driest extreme, and *Eleocharis* and *Luziola* species in the more humid areas ([Carnevali 1994](#)).

Regarding soil capacity use, Empedrado department has 38400 ha (18.9%) of arable land that can be used for agriculture with some limitations due to erosion risks. These soils are mainly located on the hills. On the other side, the biggest share (76.3%) corresponds to non-arable land located in plains. They are mainly used as rangelands, where the excess of water and reticular erosion are the main limitation factors ([Escobar et al., 1996](#)).

At a landscape analysis scale, grasslands are influenced by livestock grazing, seasonal drought and fire. Cattle, sheep and horses are the dominant livestock grazers, with cattle representing the biggest share. Fire is often used at the end of the winter to eliminate the senesced material. This tool is

sometimes used many times during the year, regardless of the season.

b. Imagery

1. Imagery and image pre-processing

Only Landsat images were studied, exact dates and other information was shown in table 1. Only one image of 27th June 2006 presented around 30% image cloud coverage, all others were cloud free images. All images were georeferenced to a rectified image of April the 02nd 2001 (UTM projection) and then strictly re-projected to TM, as making images comparable will facilitate further studies in the future.

Table 1. Scenes and registration characteristics of the used images.

acquisition date	path/row	source	satellite/ sensor	number of GCPs*	RMSE °
03 March 1987	226/079	EarthSat/GLCF ¹	Landsat 5/TM	-	orthorectified
06 September 2000	226/079	EarthSat/GLCF ¹	Landsat 7/ETM+	33	0.5033
12 January 2001	226/079	CONAE/INTA ²	Landsat 7/ETM+	33	0.3279
02 April 2001	226/079	EarthSat/GLCF ¹	Landsat 7/ETM+	-	base Image
15 January 2002	226/079	CONAE/INTA ²	Landsat 7/ETM+	33	0.2938
17 December 2002	226/079	CONAE/INTA ²	Landsat 7/ETM+	33	0.2319
24 April 2003	226/079	CONAE/INTA ²	Landsat 7/ETM+	33	0.2492
08 August 2004	226/079	CONAE/INTA ²	Landsat 5/TM	33	0.2303
20 March 2005	226/079	CONAE/INTA ²	Landsat 5/TM	33	0.3966
27 July 2006	226/079	CONAE/INTA ²	Landsat 5/TM	22 ³	0.3875

* ground control points

° root mean square error

¹ Comisión Nacional de Actividades Espaciales / Instituto Nacional de Tecnología Agropecuaria

² Global Land Cover Facility

³ less GCP because of cloud cover interference

The final projection was set as:

Projection type: Transverse Mercator
Spheroid name: WGS 84
Datum name: WGS 84
Scale factor at central Meridian: 1000000
Longitude of central Meridian: 57:00:00.00000 W
Latitude of origin of projection: 90:00:00.000 S
False easting: 6500000 meters
False northing: 0.0000 meters

For georeferencing 33 GCP were used each time (the final RMS errors were shown in table 1).

The spectral values for each pixel were interpolated using a nearest neighbour resampling approach. Data were output to a 28.5 x 28.5 m pixel size. All images were subset to the Empedrado political boundary.

2. Imagery normalization

All Landsat images were normalized to the one of 17th December 2002. The normalization procedure has been reported to be necessary in multitemporal studies to ensure comparability between images and classification reliability ([Paolini *et al.*, 2006](#)). Additionally, it is known that a common radiometric response often is required for quantitative analysis of multiple satellite images ([Hall *et al.*, 1991](#)). Therefore, the linear scale invariance of the multivariate alteration detection (MAD) transformation was used to obtain invariant pixels for the automatic relative radiometric normalization ([Canty *et al.*, 2004](#)). This method normalizes images with the same area and same spatial resolution. It uses pixels whose reflectance is more or less constant with time. The so called pseudo-invariant features (PIFs) are pixels spectrally stable over the time. This method has the advantage of objectively choosing PIFs and thus avoiding a subjective and tedious visual inspection.

The normalization process was done with ©ENVI + IDL 4.2 software by

following the ordinary least squares regression method. After obtaining the intercept “a” and slope “b” values of a linear projection for each band, a simple model was developed with ©ERDAS Imagine software ([ERDAS 1999](#)) and applied individually to every band on each image (appendix A, table 1 to 9 show the normalization parameters).

On the one hand, NDVI was calculated from the following cloud free images, September the 06th 2000; January the 12th 2001; April the 02nd 2001; December the 17th 2002 and April the 24th 2003 (table 1). Cloud free images are those in which no clouds are visible or not recognizable. NDVI was calculated not only from radiometrically normalised images, but also from not radiometrically normalised images. Each pair of historic NDVI values was then plotted.

Additionally, one MrSID (multiresolution seamless image database) compressed image of July the 27th 2006 was used for the field campaign. This format was used as reported as essential for large images. It allows much higher compression ratios than other methods ([ERDAS 1999](#)). ©Arc Pad software version 6.0 was used during the field work.

3. Vegetation indices

Normalised difference vegetation index

The Normalised Difference Vegetation Index (NDVI) was calculated from satellite imagery. For that reason, the digital values corresponding to the reflectance in the red (R) Band 3 (0.63-0.69 μm wavelength) and near-infrared (NIR) Band 4 (0.76-0.90 μm wavelength) of Landsat were used.

$$\text{NDVI} = (\text{NIR} - \text{R}) / (\text{NIR} + \text{R}) \quad (1)$$

Soil-adjusted vegetation index

The soil-adjusted vegetation index (SAVI) was calculated from the Landsat image on 27th of July 2006. For that reason, the digital values corresponding to the red (R) Band 3 (0.63-0.69 μm) and near-infrared (NIR) Band 4 (0.76-0.90 μm) were used to calculate the index in the following way:

$$\text{SAVI} = \{(1 + L) \times (\text{NIR} - \text{R})\} / \{(\text{NIR} + \text{R} + L)\}, \text{ where } L = 0.5 \quad (2)$$

4. Biomass estimation

The historical total dry matter yield (DMY) data, starting in 2000 was provided by the National Institute of Agriculture (Corrientes - INTA). Only data between 2-10(13) days after and before the satellite overpasses were used (appendix B, fig. 1). The historical data belongs to studies conducted by the forage group within the frame of the cattle raising experimental system. Measurements had been taken on grasslands located in different paddocks in the Corrientes Experimental Station (INTA). The experiment consisted on several transects located in 3 different paddocks, A30 in a plain area with reticular erosion, and paddocks A63 – A67 in hilly area with no visible erosion pattern (appendix B, fig. 2). During that experiment the stocking rates varied between 0.4 and 0.8 A. U. ha^{-1} . This characteristic, ranging from less intensive to intensive grazing pressure, was thought to be enough representative of different management in Empedrado. The historical data had been collected every 20 (A67) to 60 meters (A63 and A30), but sample points not geographically located at every station. Since only the start and finish geographic location were provided, average biomass were calculated along each transect. Further details of paddock management are given in [Arias Mañiotti et al.](#) (2003) and [Goldfarb et al.](#) (2003)

The average NDVI was calculated with the ©ERDAS AOI (area of interest) tool. On each image and paddock, NDVI was averaged over an area of the total transect length and 30 meters width. After gathering all coincident biomass data and NDVI values, a simple regression equation was calculated in order to establish the relationship between both variables.

5. Land cover classification

Supervised classification

In a first step, the following five images were selected, 03rd of March 1987, 02nd April 2001, 17th December 2002, 08th August 2004 and 20th March 2005. The idea was to evaluate which image could be considered an average image, and to test which image could properly and accurately represent the land cover in Empedrado. The normalised images were classified in five major classes, using maximum likelihood statistic-based classification algorithm (©ERDAS Imagine software). The same AOI's were used for every single class in the classification process, and for each single image.

In a second step, two images were selected from the previous set for further classification refinement. Therefore, the bi-temporal analysis included one image corresponding to a dry period (March the 20th 2005) and the other corresponding to a wet period (December the 17th 2002). In addition, since fully plant coverage is normally achieved during summer season, both nearly summer images were used expecting better classification results. The process consisted in stacking bands to create two new images. One was a 6-band image combination (B3, B4 and B5 for each date) and the other was a 12-band image (B1, B2, B3, B4 B5 and B7 for each date).

In a third step, by using previous knowledge and image analysis, training areas were selected. Both images were classified in detail and two maps were obtained. After that, non-site specific areas were calculated and compared. The latter means that areas of each category are computed without regard to the locations of these areas ([Congalton et al., 1999](#)).

Finally, the classified image with better visual output result was derived to a knowledge based decision tree, by integrating ancillary data (fig. 5). For that reason, a soil shape file (layer in GIS with additional geographic information), a crop shape file, the vegetation type and the current management (derived from ground truth information) were used.

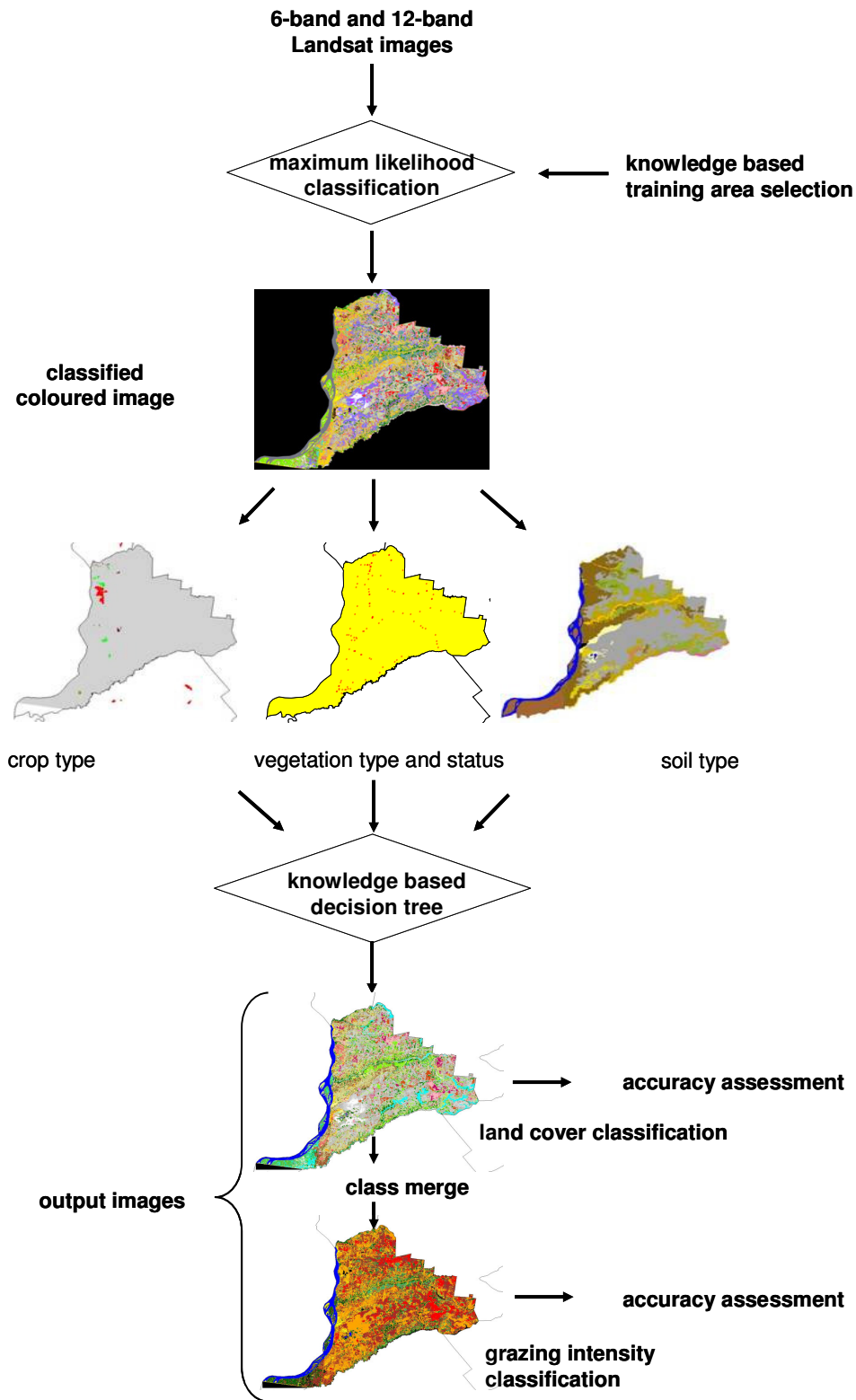


Figure 5. Schematic representation of the classification showing the integration of multi-band imagery and ancillary data.

Soil and crop information was provided by Corrientes INTA – Recursos Naturales). Additionally, ground truth data were collected during the field campaign not only helped to make sure that the training samples were correctly selected, but also to re-arrange and discriminate overlapped classes.

Last but not least, starting from the 26-class map, a second 8-class thematic map was obtained by merging classes with similar grazing intensity (fig. 5).

Accuracy assessment

Accuracy assessments were done to test the reliability of the two generated classifications. Completely random reference points for the assessments were generated with ©ERDAS Imagine. The former were not stratified to avoid introducing possible biases. For both classifications overall accuracy, kappa coefficient, users' and producers' accuracy were derived.

In this study the assessments were based on random procedures and therefore not all classes had the same size, as the number of samples can be adjusted according to the relative importance of the category ([Congalton et al., 1999](#)). Less important classes had less samples and *vice versa*. Besides that, some classes were even not even sampled (appendix H, table 28). For the integrated land cover classification, a total of 1385 reference pixels were used, while 268 for the grazing intensity classification. An average of 53 and 33 points per class were used respectively. Previous knowledge, ground truth data and sometimes ©Google Earth was used as source of reference data for the accuracy assessments.

Legend generation

The legend was built following the Land Cover Classification (FAO-LCCS) approach. Accordingly, LCCS software version 2 was used. LCCS is an objective, partly dichotomous, modular-hierarchical approach. It is a comprehensive standardized classification system, designed to meet specified user requirements, independent of the scale or means used ([Di](#)

[Gregorio et al., 2005](#)). It is stressed that the attempt to map land cover goes beyond a simple physiognomic map, since it includes several additional features. For a more detailed explanation see [Di Gregorio loc cit.](#)

6. Stocking rate calculation

To calculate provincial and departmental stocking rates, animal units (A. U.) system and adjusted grassland area were utilised. A. U. equivalences were shown in appendix G, table 26. The adjusted area was also calculated by extracting all non-grassland areas from the total grassland cover. Moreover, different percentage of available grazing resource area was considered (appendix G, table 27). Similar consideration was followed by [Deregibus](#) (1988) who indicated that for example forests offer only 50% of grass resource and savannas up to 75% of the available area.

The grazing influence of horses, sheep and goats, was not considered on the calculations, because of lack of precise information.

c. Ground truth data collection

1. Experimental design

Two experimental sites were placed in two different landscapes / locations. The first one located in the hilly area at the INTA Corrientes Experimental Station and the second one in a private property close to Empedrado city (owned by Mr. Osvaldo Vallejos) located in the vast plain area. The field sampling period was during the southern hemisphere winter. This period was chosen to coincide with the satellite overpasses after a detailed analysis of the Landsat acquisition calendar ([USGS](#)).

For site characterization and biomass calculation a field experiment was designed. The experimental unit was a nine block design (28.5 m x 28.5 m for

each block) and five sampling locations within. Square blocks were used because according to the [environmental resource team](#) (1994), in general, this shape yields better results for plant surveys. An attempt was made to sample all 90 points within 8-day period to minimize the effect of vegetation change. Each one was predetermined using randomly-selected grid coordinates generated with ©Microsoft Excel software in the lab. In the field, x and y coordinates were placed out from an appropriate axis in meters. Five samples were taken and each sampling position was geographically collected with GPS.

In every sampling point the following attributes were recorded, floristic composition (BC) by the dry weight rank method (DWRM), visual estimation of percentage of standing dead material (SDM), percentage of mulch (M) and percentage of bare soil (BS). No ocular biomass estimates were taken because the training process would have taken too much time to be accurate enough. Additionally, total aerial biomass was gathered by clipping on 0.25 m² quadrates and nineteen oven dry compound samples were calculated for each block. Only grass share was chemically analysed, carbon, nitrogen and protein content was determined.

2. Laboratory evaluations

The clipped vegetation samples were classified into major plant components (*graminoids*, *cyperacea*, *legumes* and *weeds*). The material was weighed and oven dried at 60° C until constant weight. Once dry, it was weighed again to obtain dry matter weight. Aerial dry biomass was calculated from the difference between wet and oven dry plant biomass.

To evaluate range condition, trend and cover index (INTECO) was calculated because it has been already demonstrated to be useful in Corrientes ([Goldfarb et al., 2003](#)). This index is calculated by summarising all the attributes recorded in the field (SDM, M, BS) and multiplied by a species quality coefficient (SQ), (equation 3).

$$\text{INTECO} = (\text{SDM} + \text{M} + \text{BS} + \text{DMY}) \times \text{SQ} \quad (3)$$

SQ is defined for each species as follows, fine = 2; tender = 1; ordinary = 0.5; hard = 0.25 and weeds = 0.1. INTECO ranges from 10 to 200.

BC, aerial dry biomass for each species, species relative frequency and INTECO were calculated based on the ©Botanal Sombbrero software (adapted by [Casco et al., 2002](#)).

3. Validation of biomass estimation

Once getting the regression equation between historical DMY data and NDVI, biomass was estimated from remotely sensed data considering NDVI as dependent variable (y), and biomass as independent variable (x). The accuracy of biomass estimates from remotely sensed images was then determined by the comparison with those values derived from field measurements. The biomass values were estimated from the NDVI of the 27th July 2006 Landsat image. In order to match NDVI and biomass data, the former were grouped by following three approaches,

- First, each biomass value was considered individually and plotted against the respective NDVI value, even though the latter presented identical values
- Next, all biomass data coincident with one pixel were averaged and plotted against the respective NDVI pixel value
- Finally, interpolated biomass values were plotted not only against NDVI, but also against file pixel values for each band

The Arc GIS Spatial Analyst software (©ESRI) was used for the interpolation procedure. A surface interpolation model was conducted on each variable using the inverted distance weight method (IDW). The latter give stronger weight to closer values and slowly diminishes the further one gets away from

the considered point. The 4 closest biomass sample points were used for IDW calculation. The other parameter, output grid cell size, was set at 1 meter to reflect field data collection variability. Interpolated biomass values were then averaged on a new cell extent of 28.5-meter block size, to reproduce the Landsat pixel. This procedure was followed for total and green biomass, for all groups (G, SDM, weeds) (see appendix E, fig. 9 and 10).

4. Landscape survey

121 previously selected points were randomly spread over Empedrado, reflecting the landscape diversity. At each site, GPS readings were collected and the following information qualitatively assessed, vegetation type, number of vegetation layers, dominant specie(s), management (grazing intensity levels), percentage of soil cover, and vegetation height. The complete field form is given in appendix B, fig. 3. Two Garmin eTrex GPS were used and 145 digital pictures were taken with a 4.0 mega pixels digital camera (Kodak).

III. Results and discussion

a. Normalized imagery

Atmospheric condition and illumination geometry, among other factors are affecting the comparability of multi-temporal images. It is generally accepted that the goal of the radiometric normalization is to remove all the mentioned effects ([Hall et al., 1991](#), [Paolini et al., 2006](#)).

Pairs of NDVI were linearly related (fig. 6) but not significantly different (paired t-test ≤ 0.01), (appendix C, table 10). It could therefore be inferred that the normalisation procedure seems not to be necessary.

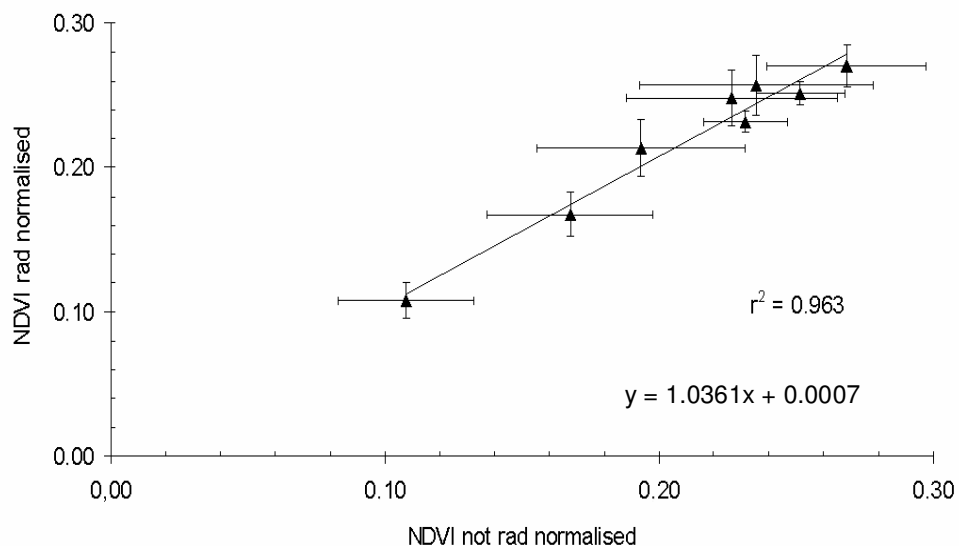


Figure 6. Plot of NDVI values calculated from radiometrically (rad) normalised and not radiometrically (not rad) normalised cloud free images. Bars indicate standard deviation.

Differently, when working with a recent cloudy Landsat TM image (2006), the normalisation was necessary. As the procedure was based on a linear relationship, the NDVI values (radiometrically normalised and not radiometrically normalised) are also linearly related (fig. 7).

But opposite to cloud free images, they were significantly different (paired t-test ≤ 0.05), (appendix C, table 11).

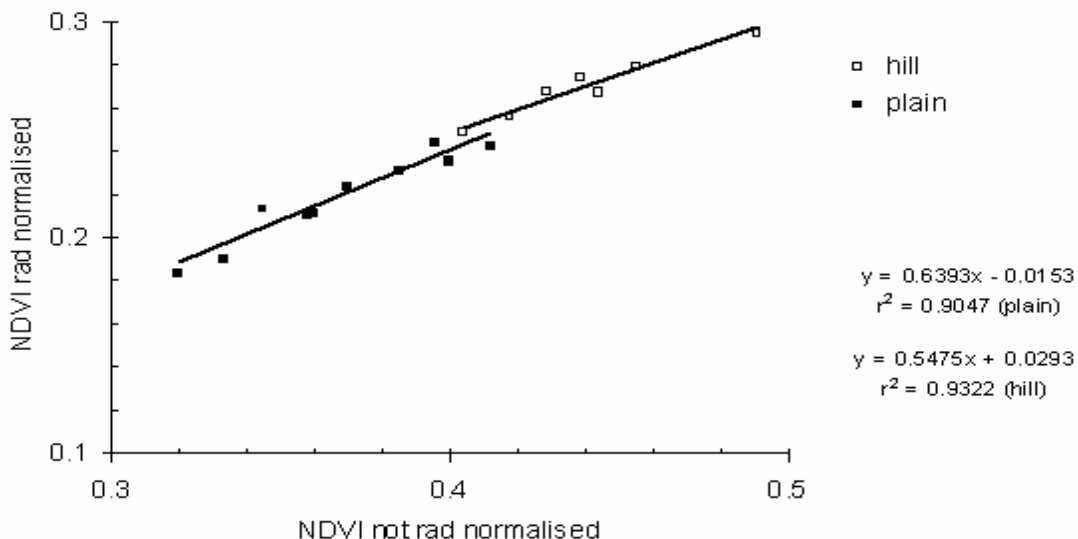


Figure 7. Plot of NDVI calculated from a (rad) radiometrically normalised image against NDVI values from a not (rad) radiometrically normalised image under cloudy conditions.

It could be concluded that NDVI's calculated from not radiometrically normalized cloud-free Landsat images would have been comparable. The additional normalization procedure was not always necessary. Time and effort could be saved, since NDVI calculation was a normalization step by itself. It must be clear, that when working with cloudy images, the normalization should be performed beforehand in order to make NDVI values comparable.

b. Site characterization and site assessments

As explained in chapter 2, two grasslands were evaluated, one on the hill, and one on the plain area. Each site was homogeneous, no significant differences within and between blocks were found tested with ANOVA ($p < 0.05$). Each site exhibited homogeneous vegetation, total biomass, SDM, total dry mater and total SGB.

When comparing differences and similarities between both sites, floristic

composition showed important differences (tables 2 and 3).

Table 2. Dry biomass on the hill site expressed as dry matter for the five principal species.

Species	kg ha ⁻¹	%
<i>Vernonia chamaedrys</i> Lees.	1775.8	50.7
<i>Sorghastrum agrostoides</i> (Speg.) Hitchc.	479.2	13.7
<i>Eryngium horridum</i> Malme	396.5	11.3
<i>Sorghastrum nutans</i> (L.) Nash	381.4	10.9
<i>Paspalum notatum</i> Flügge	130.1	3.7
Total*	3496.8	100.0

(*) total aerial biomass. For a complete list see appendix D, table 24.

V. chamaedrys and *E. horridum* are non palatable.

Sites were significantly different regarding INTECO, NDVI; SDM and total biomass (kg ha⁻¹), but no significantly different regarding BS and M (p<0.05, appendix C, tables 12 to 17).

Table 3. Dry biomass on the plain site expressed as dry matter for the five principal species.

Species	kg ha ⁻¹	%
<i>Paspalum intermedium</i> Munro ex Morong et Britton	1037.5	45.4
<i>Sorghastrum agrostoides</i> (Speg.) Hitchc.	611.4	26.7
<i>Andropogon lateralis</i> Nees	418.8	18.3
<i>Axonopus affinis</i> Chase	56.2	2.5
<i>Paspalum urvillei</i> Steud.	38.8	1.7
Total*	2271.6	100.0

(*) total aerial biomass. For a complete list see appendix D, table 25.

Grasses were the dominant group not only on the hill, but also on the plain site (appendix D, tables 22 and 23). But, regarding biomass share, grasses represented the biggest portion on the plain site, and weeds represented the biggest share on the hill site, (appendix D, tables 24 and 25). Although useless for animal production, the weed biomass may provide useful information on detecting degradation processes.

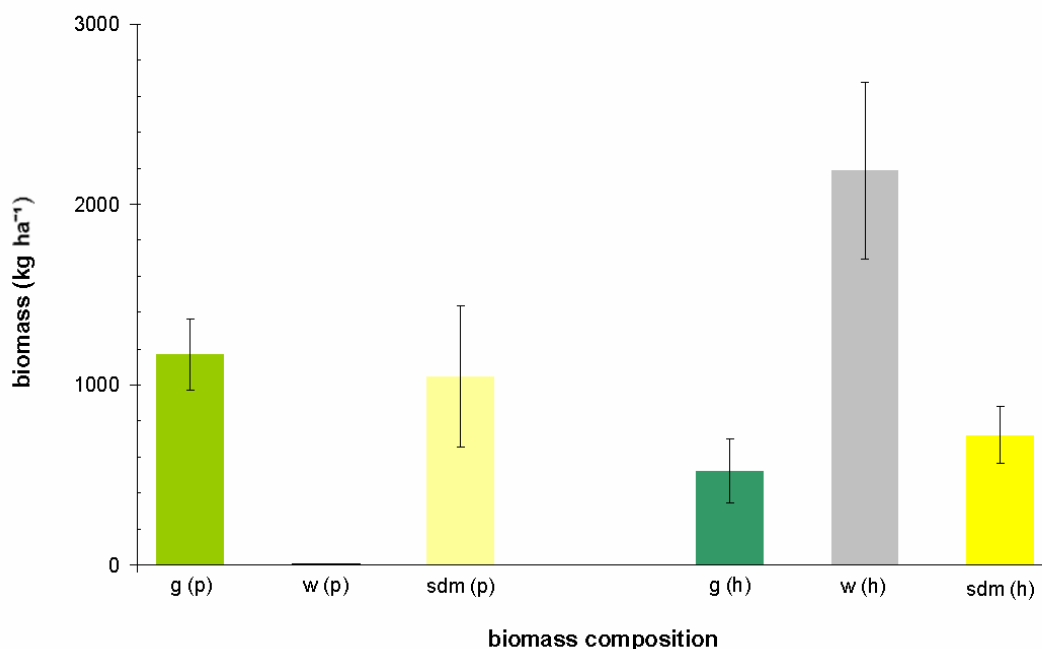


Figure 8. Biomass composition expressed as kg of dry matter per ha⁻¹, g = grasses, w = weeds, sdm = standing dead material, h = hill, p = plain. Error bars indicate standard deviation.

It has to be considered that the current studies were done during winter, when low growth rate occurs. On hills, a high portion of grass biomass was already removed by cows, whereas weeds remained not consumed hence representing more than 50% of total biomass. On plains, an important proportion of present biomass was found unconsumed as SDM (fig. 8). Field data set also indicated that the high proportion of non-edible weeds, which remained green on the hills, increased the NDVI values. On the contrary, on the plain site, weeds were hardly found, and lower NDVI and higher INTECO values were registered (tables 2, 3 and 4, figure 8). This relationship should

be investigated further in the future by analyzing more images and field sites. It may provide a tool to identify those paddocks that have been efficiently grazed or those paddocks which are being used at an extreme point where just weeds are dominating.

Table 4. Average INTECO and average NDVI calculated from current winter data sets

	NDVI	Sd	INTECO	Sd
hill	0.269	0.012	24.3	6.1
plain	0.220	0.019	34.4	3.0

Sd = standard deviation

Regarding SDM, it was found that on the plain site the SDM was higher than on the hill site (fig. 9). On the plain, SDM was almost totally represented by grasses and therefore it increased INTECO values, showing better range condition and better feed quality, but NDVI remained lower than on hills. Both variables were positively related (fig. 9).

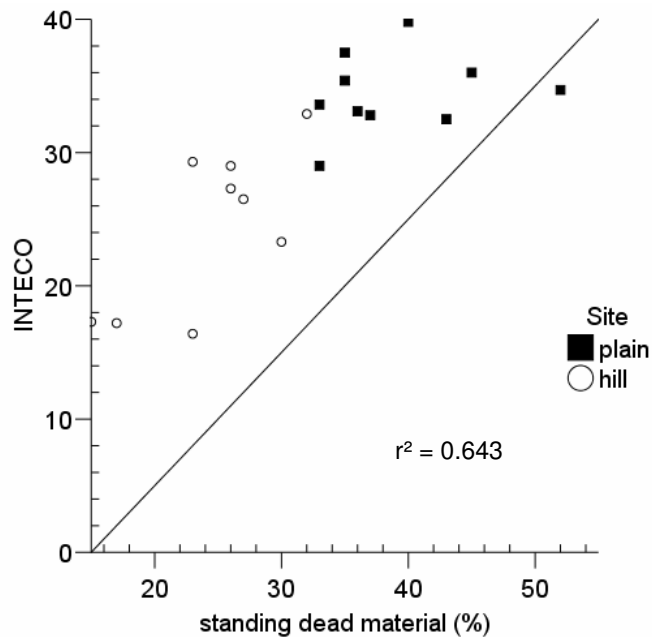


Figure 9. Relationship between INTECO and SDM. Solid line indicates the 1:1 relationship.

No significant differences in protein content of grasses were found between the hill and plain sites. It was mainly due to the similar forage species composition. Regarding carbon content, significant differences were found ($p < 0.05$), (appendix C, tables 18, 19 and 20). As protein content was low, and higher amounts of SDM were found on plains, the grassland resource could be improved there, by adding external protein sources (like urea), to increase the consumption of livestock [Deregibus 1988](#).

Table 5. Comparison between BS and M on hills and on plains.

	BS (%)	<i>Sd</i>	M (%)	<i>Sd</i>
hill	22.8	4.6	12.0	5.6
plain	19.9	5.7	13.6	7.1

Sd = standard deviation, BS = bare soil, M = mulch

[He et al., 2006](#) found that BS and soil cover had strong influence on the reflectance pattern when trying to estimate biophysical characteristics of the vegetation. In the present study, both calculated variables, M and BS were not significantly different ($p < 0.05$) on hill and plain sites (appendix C, tables 13 and 15). The same spectral influence should be attributed to BS and M, since in both sites the proportions were similar. BS and M represented below 23 and 14% (table 5), it can be inferred that they had no influence on the calculated indices. Additionally, when plotting biomass against the two vegetation indices (NDVI and SAVI), both were slightly linearly related to biomass, but no significant differences were found when using either one or the other (fig. 16 and 17).

c. Assessments working with historical data

Historical data also showed that NDVI and INTECO were inversely related. Higher NDVI were frequently recorded on hills, while lower on plains (fig. 10 A - B). Even though the relationship was not strong ($r^2 = 0.45$), the satellite evidence supports the suggestion that unconsumed green weed biomass

increases NDVI values on hills. Care should be taken when trying to infer biomass from satellite calculated NDVI and use it for range management, since not all biomass is digestible.

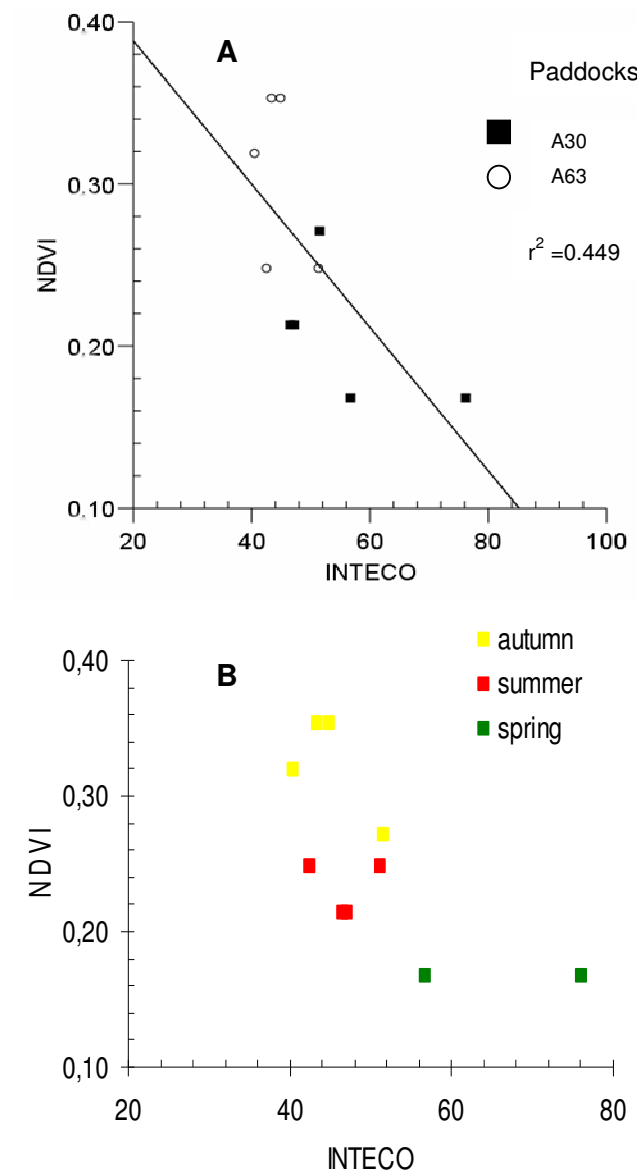


Figure 10. Relationship between INTECO and NDVI calculated from historical data sets. A, shows different paddocks, and B shows different seasons.

d. Relationship between biomass and vegetation indices

1. Historic data

Historical data exhibited that the relationship between total rangeland biomass and NDVI was linear and positive (fig. 11). Moreover, when NDVI values were plotted against historical biomass averages NDVI could explain only 50% of the total biomass in rangelands.

When compared separately, the relationship was found to be far better in hills than in plains, with $r^2 = 0.76$ ($n = 6$) and $r^2 = 0.18$ ($n = 4$) respectively, but statistically weak because of insufficient data. This relationship between NDVI and total grasses biomass considering both sites, hills and plains, separately was graphically represented in appendix E, figs. 4 and 5.

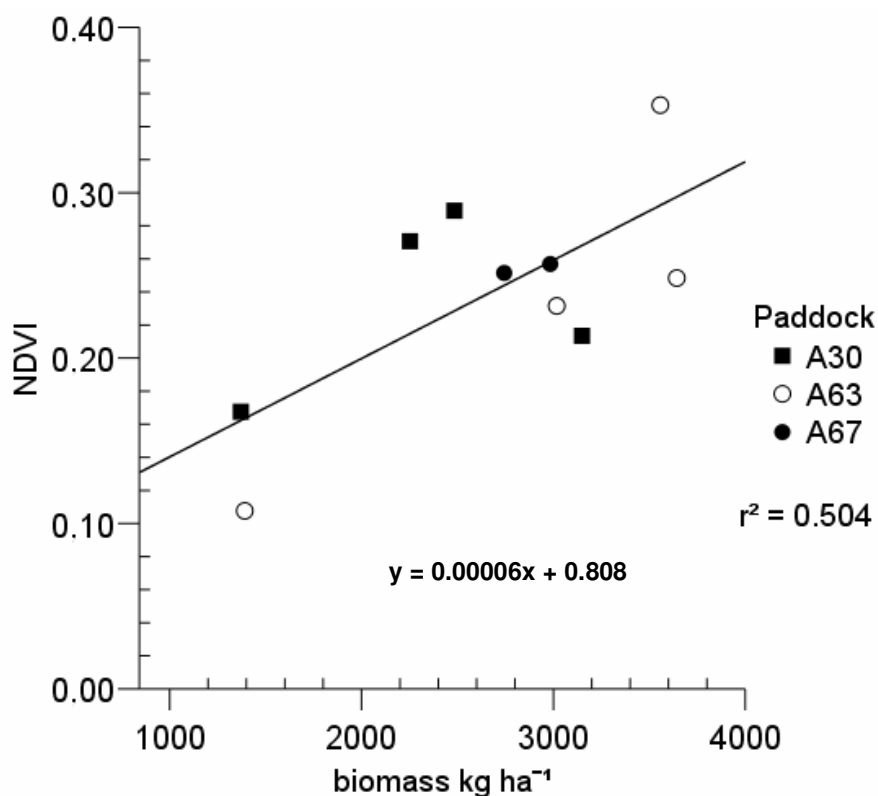


Figure 11. Relationship between total biomass, expressed as dry matter, and NDVI. A30, A63 and A67 are different paddocks.

Even though the relationship between biomass and NDVI was linear and positive, it was developed by using total biomass and not only green biomass.

The current spectral response, caused by mixed green and senesced material, was a problem that could not be addressed, and was therefore attempting for a stronger relationship.

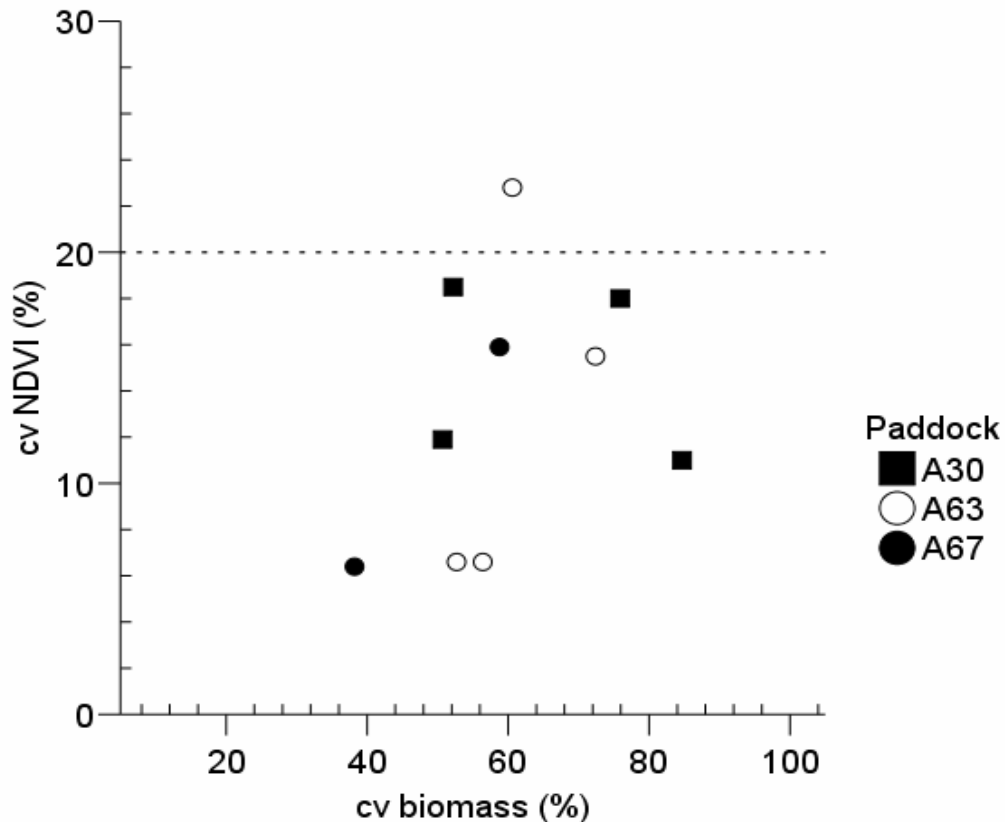


Figure 12. Relationship between C. V. of total biomass and C. V. of NDVI. A30, A63 and A67 are different paddocks where measurements were done.

The spatial heterogeneity of total rangeland biomass was higher than the variability represented by the NDVI values (fig. 12). This huge variability, explained by the C. V. of biomass data could be attributed, first to the grassland sward condition and spatial biomass variation (fig. 1). Second, historical DMY data collection did not include the separation of standing dead material (SDM) and standing green biomass (SGB). Third, as long as biomass was clipped every 30 to 60 meters along transects, sometimes only one or two biomass data corresponds to one NDVI value. Another source of variation was the coincidence of satellite imagery and ground truth measurements. The time lag was between 2-10(13) days after and before the satellite overpasses,

and not between 5 days, as it was indicated to give accurate biomass estimations on pastures (Kelly *et al.* 2003). Finally, the considered grasslands had no clear dormant season, representing an additional source of variation.

For example, depending on climate more or less green leaves were active or not. So far, even though all C. V. were very high, the highest biomass variation was registered when dealing with autumn data and the lowest with winter data. Interestingly all C. V. of NDVI values were found to be very low and similar in all seasons, but spring (fig. 13).

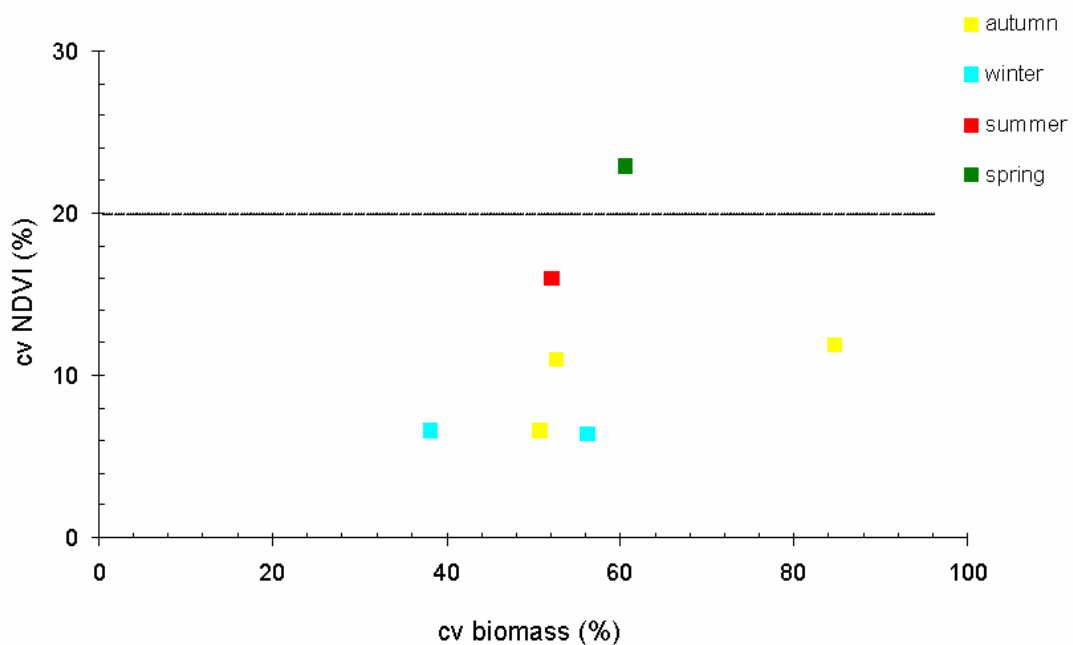


Figure 13. Plot of the coefficient of variation of NDVI against the C. V. of biomass values in different seasons.

2. Current data

With data sets collected on the field it was intended to test biomass estimations from satellite NDVI. The idea was to capture the biomass variation of the vegetation in 812.25 m² (28.5 x 28.5 m). But, even though the imagery was accurately georeferenced (table 1) the overlap was not exact enough for a perfect match. Therefore, a variable set of field biomass data

corresponded to each NDVI value, depending on its location on the image.

Rangeland biomass variability was very high inside each block. If only SGB was considered, the C. V. dropped from 84% to 75% for the hill site and from 103% to 95% in the plain site, indicating that only a small variation could be attributed to the SDM. Therefore, other factors, like management, may be responsible for that strong biomass variation.

Logically, it may be said that it would be necessary to take infinite samples in order to reduce the mentioned variability, but it was not realistic. Therefore, a compromise between the amount of field measurements and the final data variation was found.

The variation of biomass collected in blocks was higher than the variation of biomass collected along transects. As the block design was proposed to reduce the high biomass variability, and since these high C. V. levels were not acceptable, no additional benefits were achieved when working with it (fig. 12). Additionally, as experienced in the field, random sampling in blocks was more complicated to establish and very time consuming. Nevertheless, blocks provide the necessary surface distribution for interpolation, while transect sampling design does not allow this possibility.

In spite of variability, biomass was regressed to NDVI, by the approaches mentioned in chapter 2 and presented as follows,

- when each punctual biomass value was plotted against the respective NDVI, no statistically significant relationship could be established (fig. 14). Our findings agreed with those of [Anderson et al. 1993](#), who also found no relationship by using the simple point approach.
- when average biomass was plotted against NDVI, also no statistically significant relationship could be established (fig. 15).
- the interpolated biomass values plotted against NDVI improved the relationship, being positive and linear, but weak (fig. 16).

- When interpolated biomass values were plotted against SAVI, the relationship was positive and linear but also weak (fig. 17).

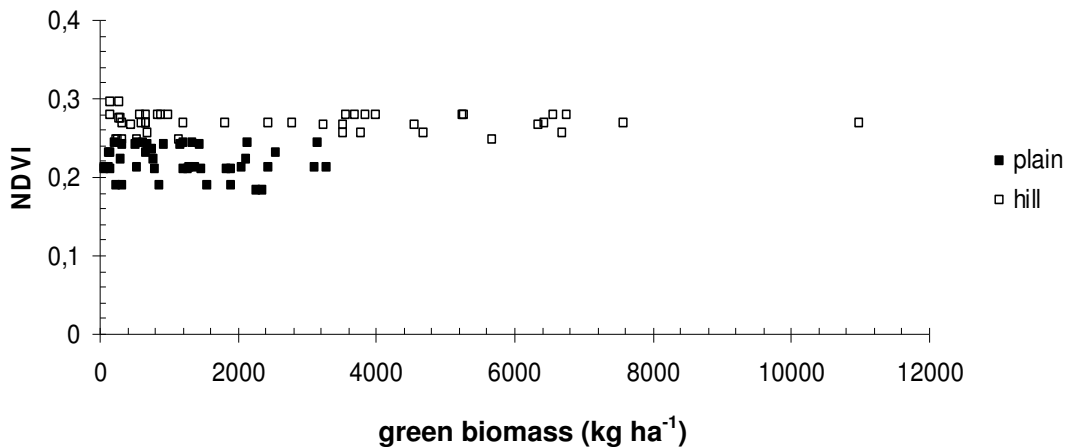


Figure 14. Relationship between NDVI and single point-biomass values.

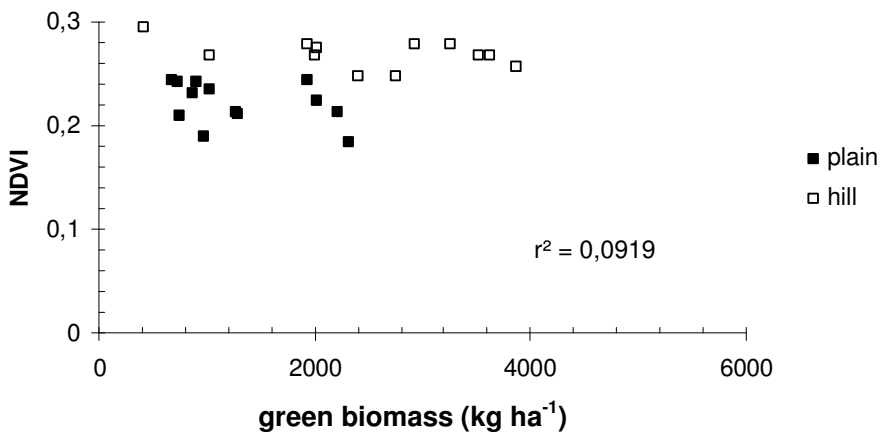


Figure 15. Relationship between NDVI and point-average biomass values.

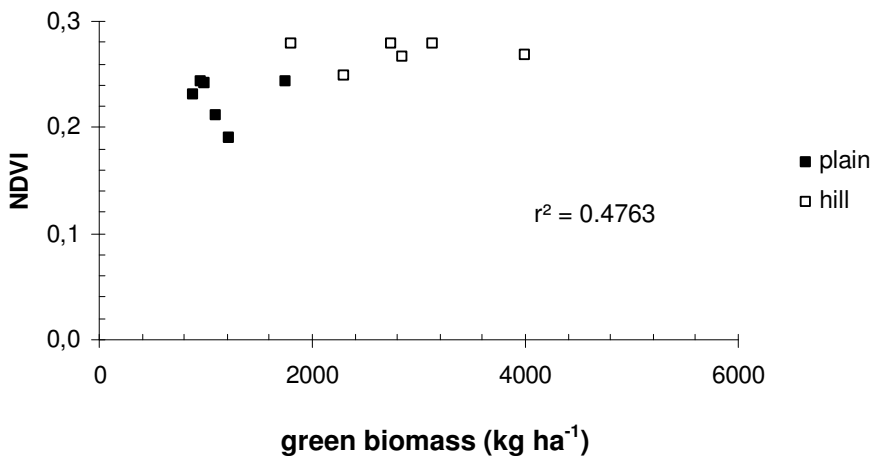


Figure 16. Relationship between NDVI and interpolated biomass values.

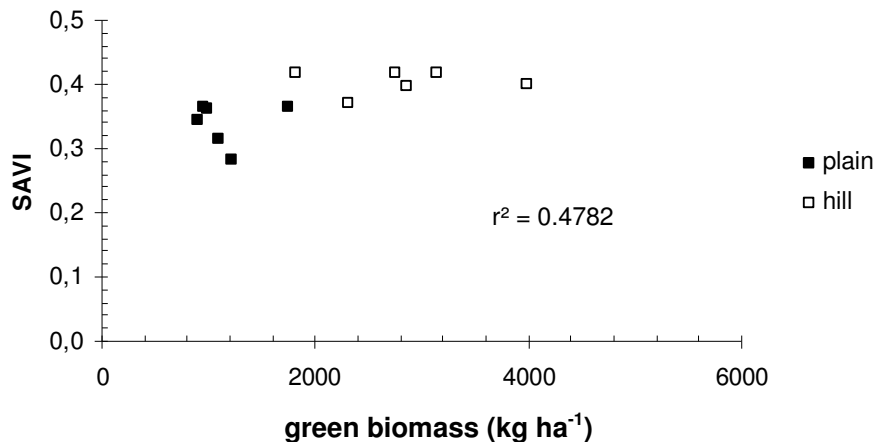


Figure 17. Relationship between SAVI and interpolated biomass values.

In summary, neither the point sample nor the average biomass did properly characterize the green biomass variability. Even though interpolated values showed better statistical fit. More data on different seasons will be needed to make stronger asseverations regarding the relationship between green biomass and vegetative indices for these and other sub-tropical grasslands.

3. Validation of biomass estimation

The empirically calculated equation (fig. 11) developed using total biomass was used for the validation. The accuracy of the biomass estimates starting from NDVI data was then tested by comparison with the values derived from on-ground measurements (fig. 18, 19 and 20).

Biomass estimates exhibited no relationship to single point as well as to average biomass (fig. 18 and 19). Current findings coincide with those of [Anderson et al. 1993](#). NDVI cannot be used as biomass estimator based on a simple point approach. But, if we consider estimates calculated by interpolation an improved estimation is achieved (fig. 20).

The advantage of spatial interpolated biomass was that the strong variability of the biomass field data was eliminated (fig. 21). Besides that, the

interpolated values could be represented as pixels of the respective image pixel and with previously decided ranges of total biomass.

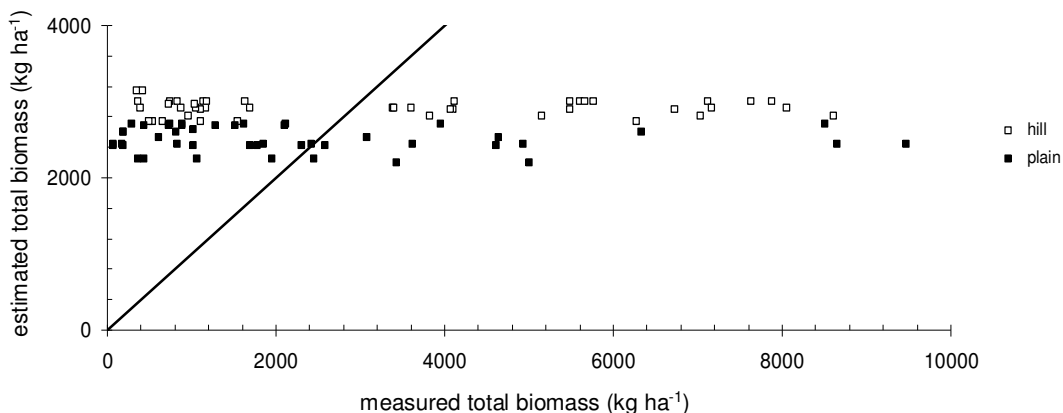


Figure 18. Estimated biomass calculated from each individual NDVI, plotted against each single measured biomass. Solid line indicates 1:1 relationship.

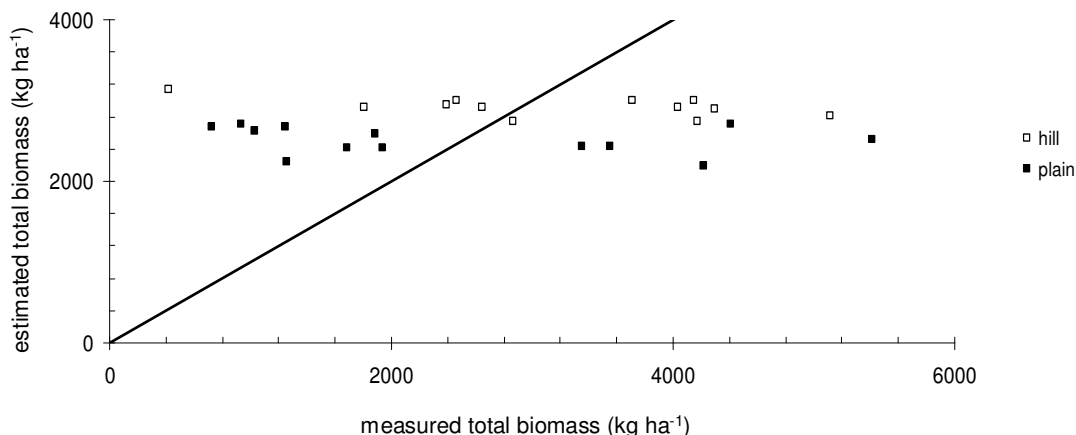


Figure 19. Estimated biomass calculated from individual NDVI, plotted against measured block-averaged biomass. Solid line indicates 1:1 relationship.

Finally, IDW interpolation gave a better idea of the reason for that variability, in other words it shows how complex was the biomass distribution on the field (fig. 21). For complete results see appendix E, fig. 9 and 10).

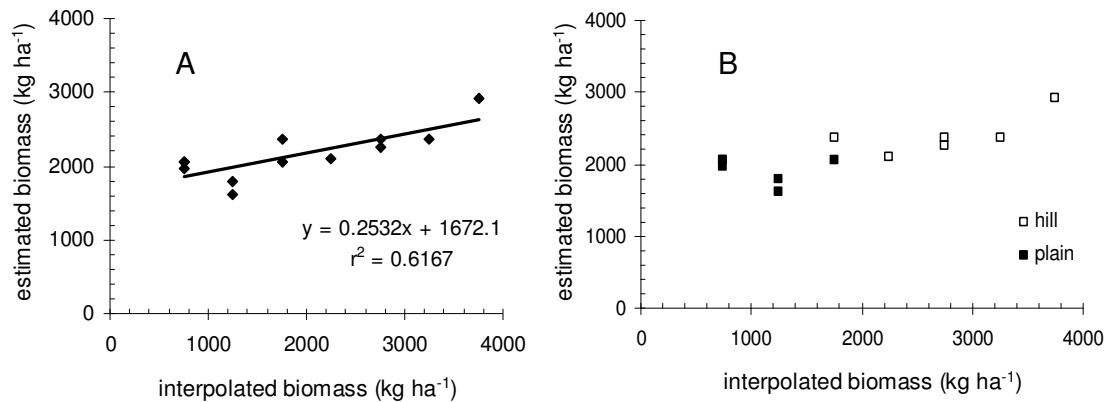


Figure 20. Estimated biomass calculated from individual NDVI, plotted against interpolated calculated biomass. Regression equation is shown in A and validation concerning each site in B.

4. Spectral characteristics of the two grassland types

Regarding reflectance for the individual bands, it was found that for band 1 the file pixel values were higher than in band 2 and 3. For band 4, higher values were found on hill than on plain, which agrees with the higher biomass on the former (SGB and total biomass), (appendix E, fig. 5). For band 5, both sites showed values similar to those on band 4. And finally, band 7 showed the highest reflectance values. Since, the difference between sites were seen for band 4, where green biomass was also high, floristic composition cannot be addressed as the only cause of this reflectance pattern (appendix E, fig. 6). No linear relationship was found between green biomass and the respective file pixel value for each band. The exception was the reflectance on band 4, with a coefficient of determination of 0.6 (appendix E; fig. 7). Reflectance on band 4 could explain the SGB levels better than NDVI.

Different to [Guo et al.](#) (2000), it could not be stated that species composition affected reflectance, since all file pixel values were very similar, but with a very different floristic composition. Besides that, the higher biomass also corresponded to a higher band 4 reflectance, which is known to be directly related to green biomass (appendix E; fig. 7).

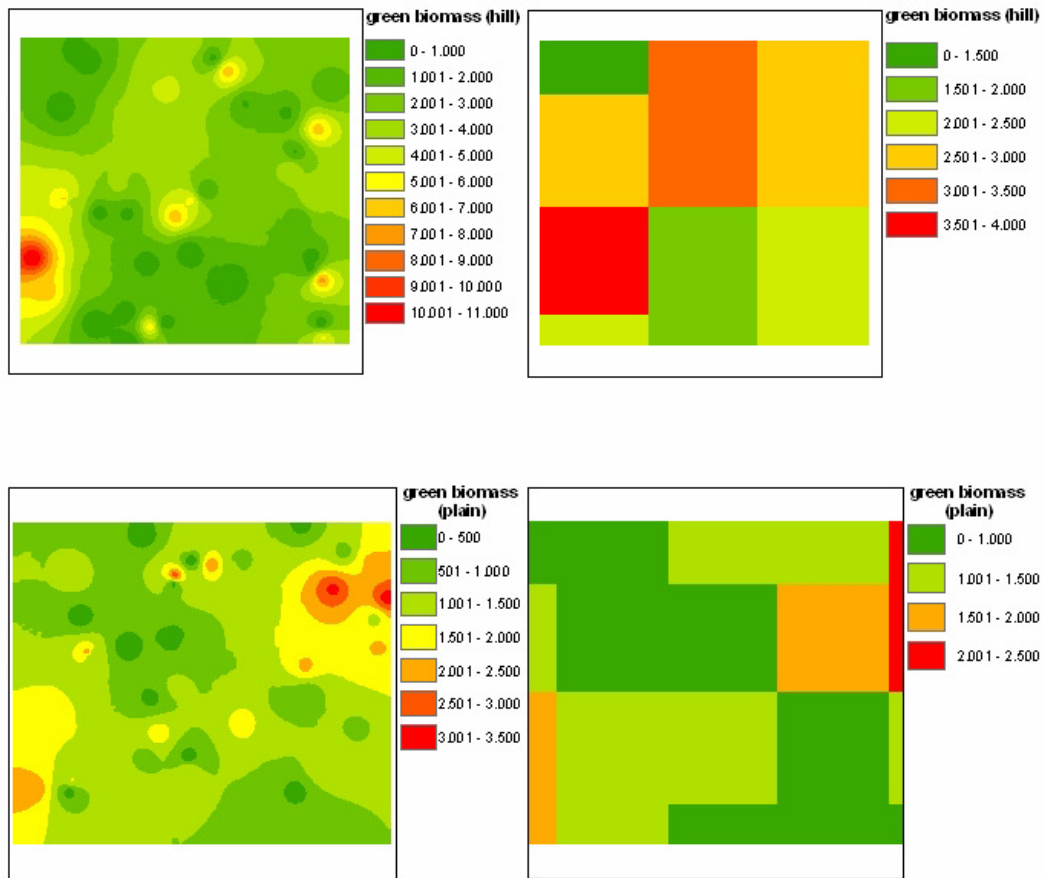


Figure 21. Grassland variability indicated by IDW interpolated green biomass values (left). Landsat pixel based interpolation of green biomass (right). All biomass values expressed in kg ha^{-1} .

e. Land cover classifications

1. Image selection

After the supervised classification, the major classes were: water, forest, marsh, grasslands in hills and grasslands in plains. The area corresponding to class “water” remained more or less constant, whilst the area of all other classes substantially changed depending on the year (fig. 22).

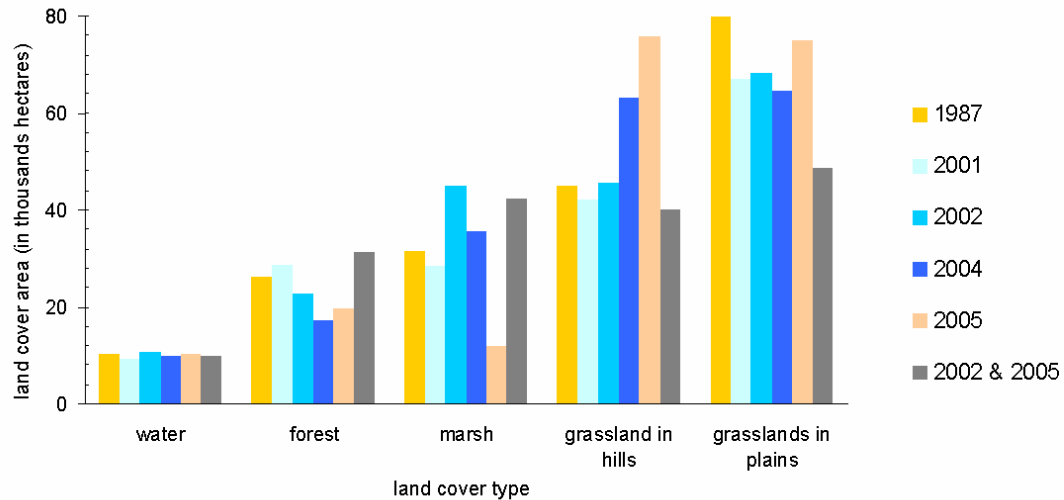


Figure 22. Major land cover classes in Empedrado department classified from satellite images. Bluish colours indicate the classified area during wet periods, yellowish colours during dry periods and grey colours indicate the final classified area including both periods (one image from 2002 and one from 2005).

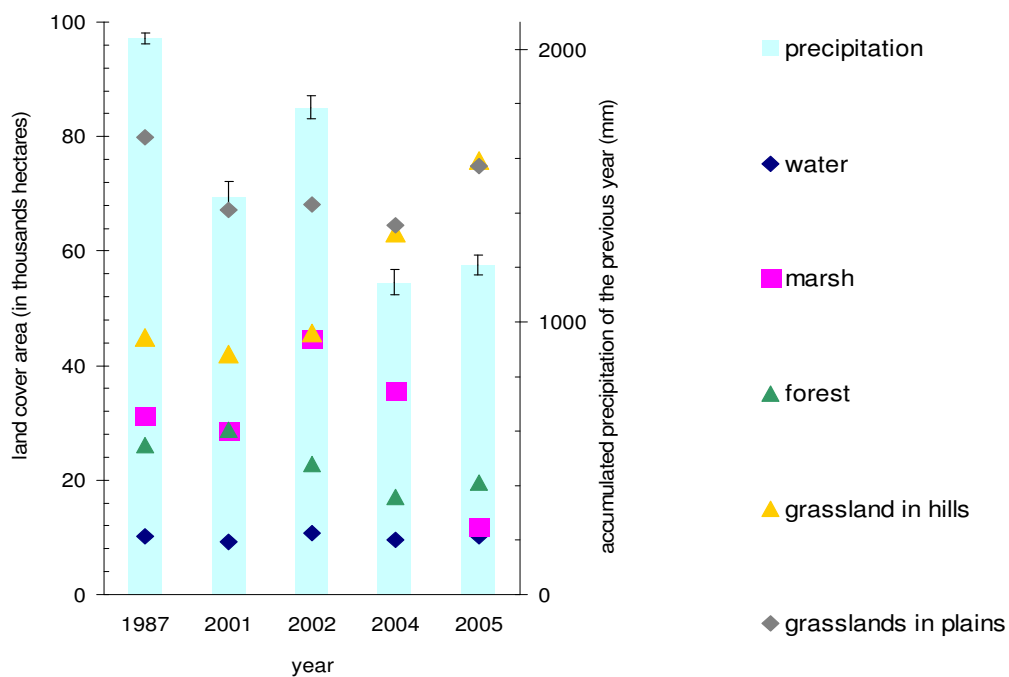


Figure 23. Relationship between occupied area of the five major land cover classes and accumulated precipitation of the previous year.

Additionally, the area of marshland strongly increased or decreased, from year to year, depending on accumulated precipitation. Similar behaviour showed grasslands in plains. In periods of low precipitation the area of

grasslands in hills increased dramatically and *vice versa* (Fig. 23).

It was demonstrated that precipitation had a major impact on classification results. This particular behaviour could be explained by the influence of the landscape in Empedrado. On plains, the general landform was represented by level land, plain and flat to almost flat terrain with smooth slopes (between 0.5 to 1%). Furthermore, the drainage was normally slowed down due to a subsurface loamy layer. On hills, the general landform was also flat to almost flat, but the slopes were between 1.5 to 3%. Therefore, water was gently discharged towards the plains. After drained to the lower areas, water remains there for longer periods ([Escobar et al., 1996](#)). Such an “average” image was not found, and spectral conditions were strongly affected by precipitation.

2. Supervised classification

After choosing two images for a detailed classification, they were stacked, as explained in chapter 2. At this point the objective was to identify and classify different land covers incorporating range use intensity levels. First, a 26-class land cover image was obtained (fig. 24). Each class had specific characteristics and can be easily compared since the FAO LCCS was used for the legend generation (table 6). For a better understanding of each class characteristics, a short description was provided in the appendix I.

Regarding grasslands, the stronger grazing pressure appeared in class 13 (short grasses-plains) and in class 16 (marsh 3), (fig. 24). Climate and topography were playing an additional important roll, since under normal or high precipitation, a layer of water allows the growth and development of palatable species ([Carnevali 1994](#)). But during drought periods, the vegetation almost disappeared under heavy livestock pressure. Besides that, intensively grazed areas were displayed as being in close geographic relationship with water bodies and other water sources.

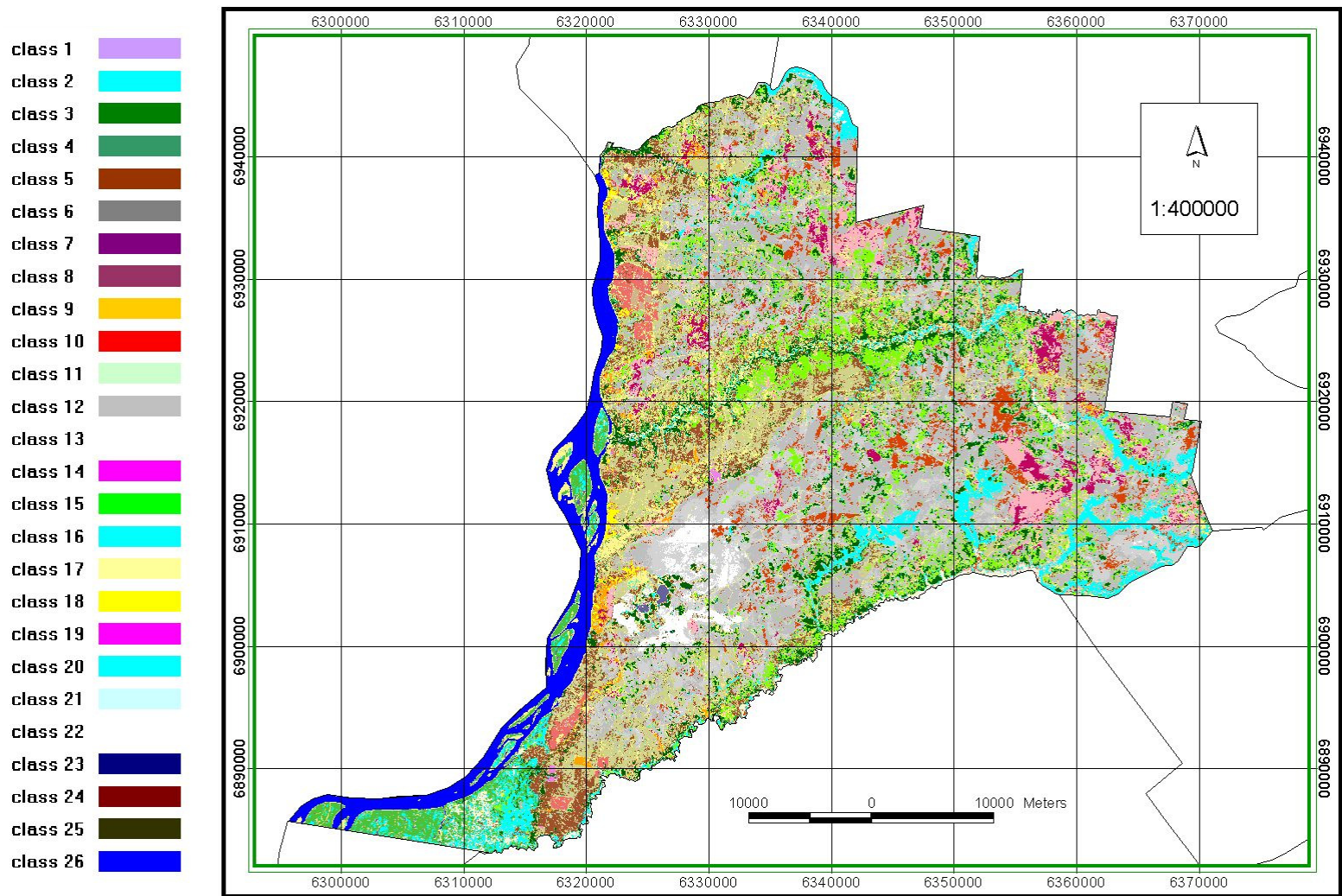


Figure 24. Map showing the integrated land cover classification for Empedrado.

Table 6. Integrated land cover classification after combining satellite imagery and ancillary data. Areas are given in hectares.

Class	Land cover classification users label	Colour	ha	Land cover classification code
1	Pastures		433	11264-S0701W4
2	Marsh (2)		2941	40838-4993-L1M251O2O15P1R1
3	Close forest		11742	20089-13180-O2O15P1
4	Close forest (2)		5110	20089-13152-L1O2O15P1
5	Grassland not overgrazed (hills)		11622	21274-12763-L1L6
6	Grassland not overgrazed (plains)		37521	21299-12132-L1M2O2O15P1
7	Grassland burned 2002 (plains)		6626	21299-12132-L1M2O2O15P1(2)
8	Grassland burned 2005 (plains)		4283	21299-12132-L1M2O2O15P1(6)
9	Grassland burned 2005 (hills)		1392	21274-12763-L1L6(3)
10	Grassland burned both dates (plains)		6432	21299-12132-L1M2O2O15P1(6)(3)
11	Short grasses - intensively grazed (hills)		23267	21303-12313-L1L5T2
12	Grassland intensively grazed (plains)		23375	21299-12132-L1M2O2O15P1(3)
13	Short grasses - intensively grazed (plains)		2890	21344-165-L1L5
14	Fallow		2017	11502-L1L6
15	Open forest		14125	20131-13233-O2O15P1Q6
16	Marsh (3)		6020	21304-12294-L1L5T2
17	Non vegetated ¹		16236	6001
18	Erosion		712	6006-L1M2O2O15P1
19	Perennial (orchards & plantations) ²		224	11342-L1W1
20	Marsh (1)		2244	40820-44920-L13R1T2
21	Water reservoir		14	7013-5-O1O15P1V1
22	Waterlogged grassland		2784	40223-4806-L1O2O15P1Q8R1
23	Lagoon		315	8011-5-O2O15P1V1
24	Rice		395	11268-13227-L1L5M2O2O15P1S0308W4X3Y4
25	Other crops		24	11223-L1M2O2O15P1S1W4X3Y4
26	River		9233	8002-1-O2O15P1V1

¹ includes roads and urban areas.

² includes citrus, pine and eucalyptus.

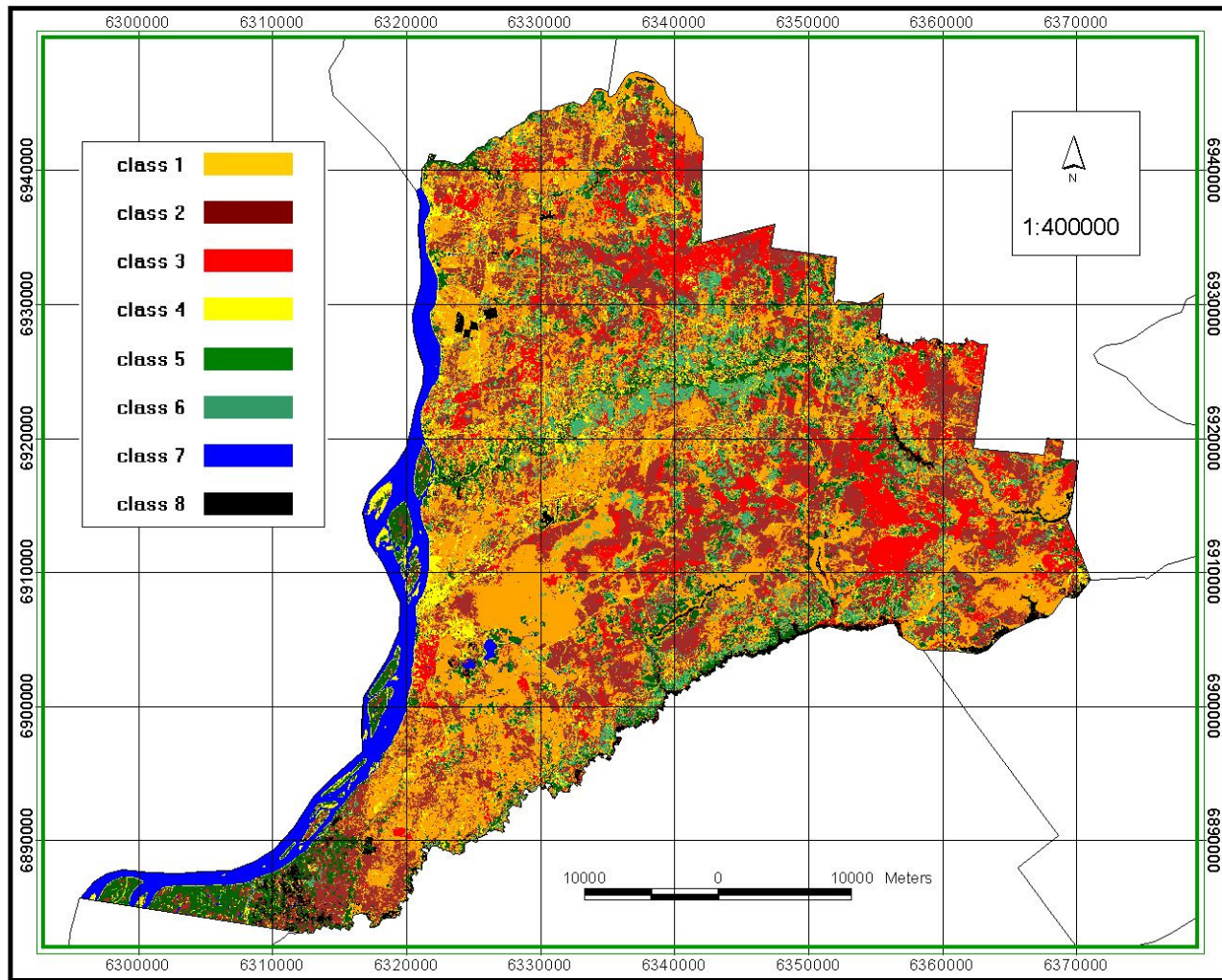










Figure 25. Empedrado's grazing pressure-land use intensity map. Blue and black classes have no grazing use, while light green and dark green colours indicate partial livestock use.

Table 7. Land cover-land use intensity classified area. Intensity levels were estimated observing grass height, grass composition and percentage of bare soil. Burned areas were identified by simple optical image analysis.

Class	Land cover / use	Colour	Area	
			ha	%
1	Intensively grazed grassland		57568	30.0
2	Not intensively grazed grassland		55301	28.8
3	Burned grassland		18733	9.8
4	Erosion / bare soil		16947	8.8
5	Forests		16851	8.8
6	Open forest		14124	7.4
7	Water		9561	5.0
8	Other		2888	1.5
Total			191973	100.0

During the field work, a better vegetation condition was found for class 16 (marsh 3) in the North-East of Empedrado where the drainages were slowed down to keep water on the fields to support continuous vegetation growth.

On the hills, class 11 (short grasses-hills), showed not only short grasses and high grazing pressure, but also some encroachment and high proportion of weeds. Class 15 (open forest) showed physiologically drought conditions, due to sodic soils (natracualf and ocracualfs), overgrazing and sheet erosion.

As explained in chapter 2, an 8-class thematic map was also obtained (fig. 25). Different classes with similar use intensity were collapsed to achieve a grazing pressure-land use intensity map. For a better understanding of each class specific characteristics, short descriptions were given in the appendix J.

For this environment, it was reported that a correct range management is difficult to achieve, since grasses are growing very fast when temperature rises and feed quality decreases quickly ([Deregibus 1988](#); [Royo Pallarés et al. 2005](#)). This mismanagement figures were now quantified for Empedrado (table 7). Results indicated that about 39% of the area was intensively grazed or had no vegetation cover, class 1 (intensively grazed grassland) and class 4

(erosion-bare soil). On the other side about 29% of the area had low grazing pressure (class 2).

Class 2 (not intensively grazed grassland) and class 3 (burned grassland) were geographically related (fig. 25). After the growing period, the area which was not appropriately grazed was normally subjected to fire to remove the dead dry material that otherwise inhibits future growth. On the opposite, areas intensively grazed of course had no dry material that could ignite a fire. Additionally, it was found that 10% of the total area was recently burned, meaning out of the “normal” fire season, which is August – September. In the mentioned areas, fire was used during December and March just when the average monthly growth rate has a maximum ([Royo Pallarés et al., 2005](#)).

Burned areas on hills were less than a tenth of burned areas on plains. Burned areas represented 22% on plains and only 1.3% on hills. Besides that, on hills 65% of the area was intensively grazed, while on plains the proportion dropped to 31%. It may be inferred that the less intensively grazed grasslands in the plains could act as a “key resource” for livestock in the winter time, as the higher SDM was found there. But, unfortunately low levels of protein concentration of about 7% (this study) may act in detriment of livestock intake. Future efforts should be devoted to a better resource use.

3. Number of bands and the roll of ancillary data

As mentioned in chapter 2, the two different supervised classifications were compared with the final 26-class image (which integrates ancillary information and which was considered as the best achievable classification). Although this analysis only constituted a non-site specific assessment, it was found that with 12 bands, 12 classes had less than 20% variation in area compared to the final classification. On the other side, with six bands only six classes presented less than 20% variation (table 8). Only classes 5, 7, 10, 15 and 26 showed less than 20% variation, independent on the amount of bands used.

Table 8. Comparison of land cover area classified using 6 or 12 Landsat bands. Ancillary data is removing the effect of evident misclassifications. Areas are given in hectares (ha).

Class	Classified area (ha)			Difference between (a) and (c) in % *	Difference between (b) and (c) in % *	
	Bands used	6 (a)	12 (b)			12 + ancillary data (c)
1		-	-	433	100	100
2		2214	2279	2941	25	23
3		8836	8942	11742	25	24
4 ¹		7209	7994	5110	-41	-56
5 ¹		11074	9632	11622	5	17
6		30126	31279	37521	20	17
7		6956	6630	6626	-5	0
8		1236	1392	1392	11	0
9		3133	4284	4283	27	0
10		6006	6434	6432	7	0
11		9379	10087	23267	60	57
12		5250	5522	23375	78	76
13		1259	1476	2890	56	49
14		27038	18783	2017	-1240	-831
15		13401	14282	14125	5	-1
16		27176	27159	6020	-351	-351
17		1183	1270	16236	93	92
18 ¹		10714	15902	712	-1405	-2134
19 ¹		83	39	224	63	83
20		3026	2670	2244	-35	-19
21		25	14	14	-78	0
22		3349	3159	2784	-20	-13
23 ¹		264	247	315	16	22
24		530	395	395	-34	0
25		3518	3083	24	-14484	-12681
26		9319	9351	9233	-1	-1

¹ in this case the classification with 6 bands returns better results than with 12 bands.

(a) 6-bands / two dates stacked image.

(b) 12-bands / two dates stacked image.

(c) 12-bands / two dates stacked image after using ancillary information.

* Percentage difference of classified area within classes.

The 12-band combination returned better results than the 6-band combination, the latter was not recommended for further classification refinement. These findings, using 12 Landsat bands (6 bands each date) coincided with those already reported for grassland classification in eastern Kansas ([Price et al. 2002](#)).

Following the previous discussion, without ancillary information the classification was far from accurate (table 8). Attempts to overcome the situation with the aid of a SRTM image failed (results not shown). Unfortunately, the differences in altitude on the field were not strong enough (less than 5 meters) to be used as an ancillary classification parameter ([Judex et al., 2006](#)). Self knowledge, a soil map and a 4-year historic crop shape file were used instead.

At the beginning several classes were partially overlapped. Only the integration of ancillary data enabled a better classification. A special issue that deteriorated the classification output was the open or sparsely vegetated soil. Classes 11 (short grazes-intensively grazed), 17 (non-vegetated) and 18 (erosion) had low vegetation coverage and therefore similar high reflectance values in the visible bands. The particularity that characterised gully erosion was that it occurred close to riversides. Riverside areas were delineated as a shape file and then used as ancillary data source. Therefore, only in this case the separation was achieved after using that self knowledge based information. Erosion (class 18) could be then easily discriminated from the other mentioned sparsely or non-vegetated areas.

After that, the soil map enabled the separation between class 3 (close forest) and class 4 (close forest 2), (table 9). Both forests had similar shape, phenology and spectral response (appendix F, fig. 11).

Additionally, classes 16 (marsh 3), 2 (marsh 2), 12 (grassland intensively grazed) and 13 (short grasses-intensively grazed) were also overlapped. The reason was that all were intensively grazed, and all had short vegetation and low vegetation coverage. Therefore all classes showed similar reflectance, easily recognizable in the 2005 image (appendix F, fig. 12). As long as the soil type was definitively different an acceptable separation was achieved (table 9). For class 16, besides to the different soils, the vegetation was also different, since grasses were not the dominant community

Class 14 (fallow) was highly overlapped with other classes, mainly with class

11 (short grazes-intensively grazed). They had a very similar spectral response in the visible and far infrared regions, particularly for the 2005 image (appendix F, fig. 13). An accurate separation was only achieved by using two different crop shape files, one for rice and one for plantations. Both had recent crop information for the last years. Class 14 (fallow) could therefore accurately be segregated from the others.

In a similar procedure, class 14 was segregated from classes 12 (grassland intensively grazed), 13 (short grasses-intensively grazed) and 17 (not vegetated) with the same pool of ancillary data. Classes 1 (pastures), 5 (grasslands not overgrazed) and 25 (other crops) were also overlapped, and were similarly separated.

Table 9. Prevailing soil types in the different areas in Empedrado.

class	prevailing soil type
3	argiudols, ocracualfs, paleudols and natracualfs
4	paleudalfts, psamacuents and ocracualfs
2	acueptes and acuentes
12	ocracualfs and albacualfs
13	albacualfs and glosacualfs
15	natracualfs and ocracualfs
16	albacualfs and saprists

In summary, in many cases a good discrimination was only achieved after using soil information in combination of crop-cover shape files. Only in one case, self knowledge was needed as a source of ancillary data for better discrimination.

4. Accuracy assessments

As mentioned, classification results strongly relied on the ancillary input data for an acceptable classification, without the former, the output map did not accurately represent the real land cover in Empedrado (table 6 and 8). Two accuracy assessments were done, as explained in chapter 2. Although time consuming, assessing the accuracy of complex multi-class thematic maps was essential for future resource management, since it provided a statistically valid score of the classification quality.

Both, users' and producers' accuracies were calculated. Users' accuracy is important because it shows how well spatial data actually represent what can be found on the ground. Producers' accuracy shows how easy a class can be mapped ([Congalton et al., 1999](#)). Ideally, both accuracies should be similar for all classes. However, they differed considerably among classes. Confusion matrices summarizing the relationship between classified pixels and reference information were given in appendix H, tables 28 and 29.

In the 26-class classification, in general the most difficult classes to be mapped were also those which were most difficult to identify when on ground (appendix H., table 28) and *vice-versa*.

Considering the 8-class classification, the lowest producers' accuracy was coincident with the highest users' accuracy (appendix H, table 29), because in class 8 (other) very different classes were collapsed. Besides that, class 4 (erosion-bare soil) showed very low users' accuracy, because it was similar to other classes which sparse vegetation (appendix H, table 29).

During the pixel based assessments, it was experienced that boundaries between classes represented an important source of errors. The harder task was to exactly conclude to which class a pixel in the border zone of two or more classes belonged. For both classifications, an overall accuracy close to 78% was achieved. The level of confidence was quite high, considering that on this environment vegetation coverage strongly varies depending on climate and weather conditions.

For a future classification, object-oriented image analysis may be useful to accurately and more objectively classify grasslands on hills and on plains. Dark background on plains during wet periods and bright background during dry periods were threatening the classification performance. In the present case, these classification problems were partially fixed by using ancillary data, but with the awareness that some additional sources of error were introduced, since soil maps and crop maps were a result of previous image analysis and visual based interpretation. Better classification results may be therefore obtained with images of better spatial resolution, and by following an object-oriented approach rather than a pixel based analysis ([Laliberte et al., 2004](#)).

f. Stocking rate calculation

Actual stocking rate was 0.69 A. U. ha⁻¹ and not 0.59 A. U. ha⁻¹ per year, if calculated without extracting all non-rangeland. Higher stocking rates were actually acting over Empedrado's grasslands over the last five years, 16% higher than those obtained if only total departmental area was considered, and 28% higher than stocking rates in Corrientes province. Nevertheless, stocking rates in whole Corrientes province were probably higher since the former calculation included only total and not adjusted area.

The real values were similar to previously reported calculations made for Corrientes ([Carnevali 1994](#)). Therefore, if actual trends continue, the previously calculated limit of potential carrying capacity of 0.9 A. U. ha⁻¹ per year ([Deregibus 1988](#)) will be achieved soon.

IV. Conclusions

Remote sensing constituted an ideal tool to be used in Empedrado's rangeland since the abundance of land and poor vial infrastructure makes this challenging technology very attractive for current and further applications.

For accurate imagery utilization, like post classification comparisons and multi temporal analysis, imagery normalization was always strongly recommended. In this work, it was demonstrated that when calculating NDVI from cloud free imagery, the normalization procedure could be avoided, since it was already implicit on NDVI calculation. Saving time was important, therefore normalization was suggested only when clouds were visible on the image.

Imagery selection for classification was a hard issue, since different bands combinations, season and topography interfered on the classification results. But, image selection had a subjective side, because the selected images were chosen from a previously given set.

It could not be said to what extend the variation in floristic composition influenced the reflectance patterns of grasslands in Empedrado. Nevertheless, species composition evaluation remains an essential tool to support the calculated NDVI by the Landsat images for an appropriate rangeland management.

The natural vegetation is neither homogeneous nor horizontally shaped. Standing biomass changed dramatically within short distances. Therefore, strong biomass variations along transects and unclassified biomass limited accurate biomass predictions from Landsat imagery.

By following a block design, neither NDVI nor reflectance on band 4, did properly explain the green biomass variation. Nevertheless, the degree of association between interpolated biomass and satellite data showed to be linearly related.

Estimates from NDVI could explain 60% of the current interpolated green biomass on rangelands. In order to achieve better regressions on per-humid grasslands, it is recommended to develop a new relationship working only with green biomass, by following a block random sampling design, on different seasons.

NDVI and INTECO indexes showed to be inversely related. This relationship should be further investigated. For an accurate estimation of range condition and to assess degradation trends, still a combination of the currently used Landsat images and ground data should be used. It would be promising to work with different satellite images, other than Landsat, with better spatial and spectral resolutions.

As the land cover classification had several classes, the use of ancillary data strongly improved the accuracy of the maps. The newly generated information may be used for better understanding of how changes in land cover affected the rangeland system.

This work intended to provide a highlight to improve rangeland management. By showing areas of low performance, burned and less intensively used areas, it is clear that they should be either corrected or devoted to activities with different environmental pressure. Besides that, as many livestock operators based their stocking rate on tradition, around 50% of Empedrado's area showed mismanagement features. For grassland to remain productive, the grazing intensity should be matched to the individual grasslands carrying capacity.

It was demonstrated that fire had bigger coverage on plains than on hills. Besides, more intensive rangeland utilization was seen on hills than on plains. Further attention should be given not only to this area, but also to some overgrazed areas in the plain, in order to assess (before it becomes irreversible) or dismiss possible grassland degradation. The possible causes of the recent system inefficiency, are may be related with the mismanagement figures shown by image classification analysis. Given the current situation, it

was suggested that the carrying capacity calculated by [Deregibus](#) (1988) should be reviewed for Empedrado, since the figures were already showing declining trends.

Even though the present stocking rate calculation did not differ substantially from estimations done before for Corrientes ([Carnevali 1994](#)), the new accurate values for Empedrado, were robust and methodologically strong, based on secondary data and remotely sensed imagery.

References

- ANDERSON, G. L., HANSON, J. D. and HAAS, R. H., 1993, Evaluating Landsat thematic mapper derived vegetation indices for estimating above-ground biomass on semiarid rangelands. *Remote Sensing of Environment*, Vol. 45, No. 2, pp. 165-175.
- ARIAS MAÑIOTTI, A. A., GOLDFARB, M. C., SLOBODZIAN, M. C., GIMENEZ, L. I. and NUÑEZ, F., 2003, Variación interanual de la eficiencia de cosecha en pastizales del N. O. de Corrientes. Método cálculo de raciones. *Revista Argentina de Produccionn Animal*, Vol. 23-1, pp. 139-140, ISSN: 0326-0550.
- BERNARDIS, A. C., FERNÁNDEZ, J. A., GOLDFARB, M. C. and CASCO, J. F., 2005, Efecto de la frecuencia de quema prescrita sobre la biomasa aérea de un pastizal. UNNE, A-031. Available online at: <http://www.unne.edu.ar/Web/cyt/com2005/5-Agrarias/A-031.pdf> (accessed 28 December 2006).
- CANTY, M. J., NIELSEN, A. A. and SCHMIDT, M., 2004, Automatic radiometric normalization of multitemporal satellite imagery. *Remote Sensing of Environment*, June, Vol. 91, No. 3-4 pp. 441-451.
- CARNEVALI, R., 1994, *Fitogeografía de la provincia de Corrientes*. INTA – Gobierno de la provincia de Corrientes, 324 pp., ISBN: 950-43-6059-9.
- CARRILLO, J., 2001, Carga animal y equivalente vaca (E.V.) Available online at: http://www.inta.gov.ar/balcarce/info/documentos/ganaderia/bovinos/cria/eq_uivaca.htm (accessed 28 December 2006).
- CASCO, J. F., GOLDFARB, M. C. and GIMENEZ, L. I., 2002, Botanal sombrero una herramienta computacional para estimar los atributos del

recurso forrajero. FCA 007, Available online at <http://agr.unne.edu.ar/Extension/Resumen/Forrajes/forr-007.doc> (accessed 02 January 2007).

CONGALTON R. G. and GREEN, K., 1999, Assessing the accuracy of remotely sensed data: principles and practices. Lewis Publishers, 137 pp.

DEREGIBUS, V. A., 1988, Importancia de los pastizales naturales en la República Argentina: situación presente y futura. Revista Argentina de Produccionn Animal, Vol. 8-1, pp. 67-78, ISSN: 0326-0550.

DI BELLA, C., FAIVRES, R., RUGET, F., SEGUIN, B., GUÉRIF, M., COMBAI, B., WEISS, M. and REBELLA, C., 2004, Remote sensing capabilities to estimate pasture production in France. International Journal of Remote Sensing, 10 December, 2004, Vol. 25, No. 23, pp. 5359-5372.

DI GREGORIO and JANSEN, L. J. M., 2005, Land cover classification system. Classification concepts and user manual, FAO, Rome, Italy, 193 pp., ISBN:92-5-105327-8.

DYMOND, J. R., SHEPHERD, J. D., CLARK, H. and LITHERLAND, A., 2006, Use of VEGETATION satellite imagery to map pasture quality for input to a methane budget of New Zealand. International Journal of Remote Sensing, Vol. 27, No. 6, March, pp. 1261-1268(8).

EDIRISINGHE, A., DONALD, G. E., HENRY, D. A., MATA, G., GHERARDI, S. G., OLDHAM, C. M., GITTINS, S. P. and SMITH, R. C. G., 2004, Pastures from space – validating remotely sensed estimates of feed on offer. Proceedings of the 25th Biennial Conference of the Australian Society of Animal Production, Animal Production in Australia, pp. 234.

Environmental resource team. Terrestrial plant community sampling, 1994, SOP 2037. Environmental protection agency, United States.

- ERDAS, 1999, ERDAS Field Guide, Atlanta Georgia, USA, ERDAS Inc.
- ESCOBAR, E. H., LIGIER H. D., MELGAR R., MATTEIO H. and VALLEJOS O., 1996, Mapa de suelos de la provincia de Corrientes 1:500.000. E.E.A. INTA - Corrientes. Área de producción vegetal y recursos naturales, 325 pp., ISSN: 1514 – 6529.
- EVANS, J. P. and GEERKEN, R., 2006, Classifying rangeland vegetation type and coverage using a Fourier component based similarity measure. Remote Sensing of Environment, Vol. 105, pp. 1-8 (Elsevier).
- EVERITT, J. H., ESCOBAR, D. E. and RICHARDSON, A.J., 1989, Estimating grassland phytomass production with near-infrared and mid-infrared spectral variables. Remote Sensing of the Environment, Vol. 30, pp. 257-261 (Elsevier Science Publishing Co. Inc.).
- FROST, B. and RUYLE, G., 1993, Range management terms / definitions. Arizona Ranchers' Management guide, 26 pp. Available online at: <http://cals.arizona.edu/arec/pubs/rmg/2. Rangeland Management /4Terms.pdf> (accessed 02 January 2007).
- GOLDFARB, M. C., ARIAS MAÑIOTTI, A. A., SLOBODZIAN, M. C., GIMENEZ, L. I. and NUÑEZ, F., 2003, Variación interanual de la eficiencia de cosecha en pastizales del N. O. de Corrientes. Método desaparición de la biomasa de forraje. Revista Argentina de Produccionn Animal, Vol. 23-1, pp.176-177, ISSN: 0326-0550.
- GOLDFARB, M. C., CASCO, J. F. GIMENEZ, L. I. and NUÑEZ, F., 2003, Evaluation of range condition under various fire regimes through a trend and cover index (INTECO). African Journal of Range & Forage Science. South Africa, A3.12 ISSN: 1022-0119. Available online at: http://www.geocities.com/bruno_herault/Durban.pdf (accessed 02 January 2007).

- GUO, X., PRICE, K. P. and STILES, J. M., 2000, Biophysical and spectral characteristics of cool- and warm-season grasslands under three land management practices in Eastern Kansas. *Natural Resources Research*, Vol. 9, No. 4, pp. 321-331.
- HALL, F. G., STREBEL, D. E., NICKESON, J. E. and GOETZ, S. J., 1991, Radiometric rectification: Toward a common response among multirate, multisensor images. *Remote Sensing of Environment*, January 1991, Vol. 35, No. 1, pp. 11-27.
- HE, Y., GUO, X. and WILMSHURST, J., 2006, Studying mixed grassland ecosystems I: suitable hyperspectral vegetation indices. *Canadian Journal of Remote Sensing*, Vol. 32, No. 2, pp. 98–107.
- HE, Y., GUO, X., WILMSHURST, J. and Si, B. C., 2006, Studying mixed grassland ecosystems II: optimum pixel size. *Canadian Journal of Remote Sensing*, Vol. 32, No. 2, pp. 108–115.
- HILL, M. J., DONALD, G. E., HYDER, M. W. and SMITH, R. C. G., 2004, Estimation of pasture growth rate in the south west of Western Australia from AVHRR NDVI and climate data. *Remote Sensing of Environment*, December 2004, Vol. 93, No 4, pp. 528-545.
- HILL, M. J., TICEHURST, C. J., LEE, J. S, GRUNES, M. R., DONALD, G. E. and HENRY, D., 2005, Integration of optical and radar classifications for mapping pasture type in Western Australia. *IEEE Transactions on Geoscience and Remote Sensing*, Vol. 43, No 7, pp. 1665-1681.
- IKEDA, H., OKAMOTO, K. and FUKUHARA, M., 1999, Estimation of aboveground grassland phytomass with a growth model using landsat TM and climate data. *International Journal of Remote Sensing*, Vol. 20, No. 11, pp. 2283-2294.
- INDEC, 2002, Censo Nacional Agropecuario 2002.

- JUDEX, M., THAMM, H. P. and MENZ, G., 2006, Improving land-cover classification with a knowledge-based approach and ancillary data. 2nd Workshop of the EARSeL Special interest group on land use and land cover, pp. 37, Bonn, Germany.
- KELLY, R., EDIRISINGHE, A., DONALD, G., OLDHAM, C. and HENRY, D., 2003, Ed.: S. Cox Wageningen academic publishers. The Netherlands. Satellite based spatial information on pastures improves Australian sheep production. Precision Livestock Farming. pp. 93-98, ISBN: 907-69-9822-1.
- KENNEDY, P., 1989, Monitoring the vegetation of Tunizian grazing lands using the normalized difference vegetation index. *AMBIO*, Vol. 18, No. 2, 119-123.
- LALIBERTE, A. S., RANGO, A., HAVSTAD, K. M., PARIS, J. F., BECK, R. F., McNEELY, R. and GONZALEZ, A., 2004, Object-oriented image analysis for mapping shrub encroachment from 1937 to 2003 in southern New Mexico. *Remote Sensing of Environment*, Vol. 93, 198-210.
- LI JIANLONG, LIANG TIANGANG and CHEN QUANGONG, 1998, Estimating grassland yields using remote sensing and GIS technologies in China. *New Zealand Journal of Agricultural Research*, Vol. 41, pp. 31-38.
- PAOLINI, L., GRINGS, F., SOBRINOS, J. A., JIMÉNEZ MUÑOZ, J. C. and KARSZENBAUM, H., 2006, Radiometric correction effects in Landsat multi-date/multi-sensor change detection studies. *International Journal of Remote Sensing*, Vol. 27, No. 4, pp. 685-704.
- PARUELO, J. M., OESTERHELD, M., DI BELLA, C. M., ARZADUM, M., LAFONTAINE, J., CAHUEPÉ, M. and REBELLA, C. M., 2000, Estimation of primary production of subhumid rangelands from remote sensing data. *Applied Vegetation Science*, Vol. 3, pp. 189-195.

- PEARSON, C. J. and ISON, R. L., 1997, Agronomy of grassland systems. 2nd edition. Cambridge University Press, 222 pp.
- PERUCCA, A. R., LIGIER, H. D., KURTZ, D. B. and MATTEIO, H. R., 2004, Relevamiento citrícola en 14 departamentos de la provincia de Corrientes. Año 2004. Ediciones INTA, ISSN: 1514-6529.
- PRICE, K., GUO, X. and STILES, J. M., 2002, Optimal Landsat TM band combinations and vegetation indices for discrimination of six grassland types in eastern Kansas. International Journal of Remote Sensing, pp. 1-12, preview article.
- ROYO PALLARÉS, O., BERRETTA E. J. and MARASCHIN, G. E., 2005, Grasslands of the world, The South American Campos Ecosystem. FAO 5, pp. 171-219. Available online at: <ftp://ftp.fao.org/docrep/fao/008/y8344e/y8344e00.pdf> (accessed 28 December 2006).
- SEYLER, F., CHAPLOT, V., MULLER, F., CERRI, C. E. P., BERNOUX, M. BALLESTER, V., FELLER, C. and CERRI, C. C. C., 2002, Pasture mapping by classification of Landsat TM images. Analysis of the spectral behaviour of the class in a real medium-scale environment: the case of the Piracicaba Catchment (12400 km², Brazil). International Journal of Remote Sensing, Vol. 23, No. 23, pp. 4985-5004.
- TUCKER, C. J., 1980, A critical review of remote sensing and other methods for non-destructive estimation of standing crop biomass. Grass and Forage Science, Vol. 35, pp. 177-182.
- TUCKER, C. J., TOWNSHEAD, J. R. G. and GOFF, T. E., 1985, African land-cover Classification using satellite data. Science, Vol. 227, Nr. 4685, pp. 369-375.
- TUCKER, C. J. and SELLERS, P. J., 1986, Satellite remote sensing of

primary production. International Journal of Remote Sensing, Vol. 7, pp. 1395-1416.

USGS web site. Available online at:

http://landsat7.usgs.gov/technical_details/data_acquisition/l5_acquisition_calendar.php (accessed 16 January 2007).

ZHA, Y., GAO, J., NI, S., LIU, Y., JIANG, J. and WEI, Y., 2003, A spectral reflectance-based approach to quantification of grassland cover from Landsat TM imagery. Remote Sensing of Environment, Vol. 87, pp. 371-375.

Appendices

List of figures

Figure 1. Relationship between available imagery and biomass historical data.....	74
Figure 2. Historical biomass measurements. Map showing the transect location.	75
Figure 3. Ground truth evaluation form.	76
Figure 4. Relationship between historical total biomass (A) and grasses (B), in the plain area and NDVI.	86
Figure 5. Relationship between historical total biomass (A) and grasses (B), in the hill area and NDVI.	86
Figure 6. Mean file pixel value for each TM band on hills and plains.	87
Figure 7. Relationship of mean file pixel value for band 4 and green biomass.	87
Figure 8. Relationship between interpolate green biomass and file pixel value for each Landsat band (except band 6), b1 to b7 stands for band 1 to band 7.....	88
Figure 9. Hill grassland variability indicated by IDW interpolated point biomass values (left) and Landsat pixel size interpolated biomass values (right).	89
Figure 10. Plain grassland variability indicated by IDW interpolated point biomass values (left) and Landsat pixel size interpolated biomass values (right).	90
Figure 11. Reflectance of classes 3 and 4 taken from training areas for supervised classification.	91
Figure 12. Reflectance of classes 2, 12, 13 and 16 taken from training areas for supervised classification.	91
Figure 13. Reflectance of classes 11 and 14 taken from training areas for supervised classification.	92

List of tables

Table 1. Radiometric calibration statistics. Reference image 021217, target image 870303.....	65
Table 2. Radiometric calibration statistics. Reference image 021217, target image 000906.....	66
Table 3. Radiometric calibration statistics. Reference image 021217, target image 010112.....	67
Table 4. Radiometric calibration statistics. Reference image 021217, target image 010402.....	68
Table 5. Radiometric calibration statistics. Reference image 021217, target image 020115.....	69
Table 6. Radiometric calibration statistics. Reference image 021217, target image 030424.....	70
Table 7. Radiometric calibration statistics. Reference image 021217, target image 040808.....	71
Table 8. Radiometric calibration statistics. Reference image 021217, target image 050320.....	72
Table 9. Radiometric calibration statistics. Reference image 021217, target image 060727.....	73
Table 10. Results of testing NDVI calculated from normalised and not normalised cloud free images.....	77
Table 11. Results of testing NDVI calculated from a normalised and not normalised cloudy image.....	77
Table 12. Results of testing grassland total biomass on plains and on hills.....	78
Table 13. Results of testing grassland percentage of SDM on plains and on hills.....	78
Table 14. Results of testing INTECO values between plains and hills.....	78
Table 15. Results of testing grassland percentage of BS on plains and on hills.....	79
Table 16. Results of testing grassland percentage of M on plains and on hills.....	79
Table 17. Results of testing grassland NDVI values between plains and hills.....	79
Table 18. Results of testing grasses protein concentration between plains and hills.....	80
Table 19. Results of testing grasses nitrogen concentration between	

plains and hills	80
Table 20. Results of testing grasses carbon concentration between plains and hills	80
Table 21. Results of testing interpolated and not interpolated biomass means.....	81
Table 22. Floristic composition on the hill site.....	82
Table 23. Floristic composition on the plain site	83
Table 24. Species biomass share on the hill site	84
Table 25. Species biomass share on the plain site	85
Table 26. Equivalence between livestock categories and animal units system	93
Table 27. Grassland resource availability for each class	93
Table 28. Accuracy assessment of the combined 26-class classification	94

Appendix A

Table 1. Radiometric calibration statistics. Reference image 021217, target image 870303

9906 training and 4954 test pixels

Band	intercept	<i>Sd</i>	slope	<i>Sd</i>	R	RMSE
1.0000	22.4720	0.1460	0.8705	0.0024	0.9638	4.1131
2.0000	29.4321	0.0909	0.7461	0.0020	0.9653	3.2054
3.0000	33.9026	0.1344	0.6670	0.0036	0.8836	4.3074
4.0000	37.8692	0.0950	0.5113	0.0018	0.9465	3.5971
5.0000	30.8430	0.1010	0.5970	0.0019	0.9522	4.1043
6.0000	17.2959	0.1239	0.8364	0.0026	0.9541	4.9574

Means

Target	55.7687	39.9972	35.0283	49.1883	46.2878	39.9409
Reference	70.9871	59.3771	57.2517	63.0157	58.4417	50.8147
Normalized	71.0169	59.2757	57.2673	63.0209	58.4776	50.7035
t-stat	-0.3891	1.8092	-0.2133	-0.0904	-0.5282	1.2070
p-value	0.6972	0.0705	0.8312	0.9276	0.5976	0.2275

Variances

Target	538.8445	406.5685	249.3907	559.2952	654.6472	640.3799
Reference	418.7400	230.0294	121.5997	154.1705	243.2513	454.5177
Normalized	408.2919	226.3478	110.9593	146.2348	233.3344	448.0163
F-stat	1.0256	1.0163	1.0959	1.0543	1.0425	1.0145
p-value	0.3740	0.5702	0.0013	0.0630	0.1431	0.6122
Wishart	693.4269					
p-value	0.0000					

Sd = standard deviation

Table 2. Radiometric calibration statistics. Reference image 021217, target image 000906

7292 training and 3646 test pixels						
Band	intercept	<i>Sd</i>	slope	<i>Sd</i>	R	RMSE
1	-8.4051	0.2144	1.0369	0.0026	0.9782	2.7940
2	-7.0231	0.2247	1.0298	0.0031	0.9679	3.1929
3	-7.6166	0.2884	1.0917	0.0046	0.9414	3.2087
4	-6.8741	0.2839	1.1159	0.0045	0.9453	2.5687
5	-14.3057	0.2656	1.2024	0.0039	0.9632	2.6507
6	-3.2975	0.1671	0.9705	0.0026	0.9748	4.0471
Means						
Target	81.3108	69.6832	61.6684	62.0538	66.2696	58.8522
Reference	76.0170	64.6862	59.7287	62.4723	65.4383	53.8497
Normalized	75.9029	64.7380	59.7040	62.3743	65.3750	53.8195
t-stat	1.7396	-0.6705	0.3113	1.5694	0.9060	0.3234
p-value	0.0820	0.5026	0.7556	0.1166	0.3650	0.7465
Variances						
Target	345.7660	307.4911	155.7959	105.5121	154.7347	669.9839
Reference	375.8093	321.3353	182.1001	131.4438	225.4770	636.6638
Normalized	371.7271	326.1027	185.6635	131.3969	223.6997	631.0603
F-stat	1.0110	1.0148	1.0196	1.0004	1.0079	1.0089
p-value	0.7416	0.6567	0.5586	0.9914	0.8112	0.7896
Wishart	579.7632					
p-value	0.0000					

Sd = standard deviation

Table 3. Radiometric calibration statistics. Reference image 021217, target image 010112

8171 training and 4086 test pixels						
Band	intercept	<i>Sd</i>	slope	<i>Sd</i>	R	RMSE
1	2.1963	0.1175	0.9142	0.0015	0.9898	2.1309
2	4.1102	0.1089	0.8891	0.0016	0.9873	2.0216
3	1.5828	0.1113	0.9462	0.0018	0.9851	1.6477
4	-2.2331	0.1036	1.0408	0.0017	0.9896	1.2696
5	-4.6180	0.0867	1.0760	0.0013	0.9937	1.2283
6	-0.4779	0.0338	1.0021	0.0006	0.9983	1.2681
Means						
Target	77.6145	66.0157	59.3155	60.5976	62.9077	42.2572
Reference	73.2132	62.7599	57.7090	60.8150	63.0497	41.8571
Normalized	73.1519	62.8019	57.7053	60.8377	63.0725	41.8694
t-stat	1.3796	-1.0080	0.1031	-0.7840	-0.8198	-0.4429
p-value	0.1678	0.3135	0.9176	0.4331	0.4124	0.6578
Variances						
Target	481.7013	377.9327	189.3651	149.4542	229.4919	939.0547
Reference	405.4853	299.8163	170.8752	161.2323	263.9439	941.5859
Normalized	402.5915	298.7263	169.5268	161.9021	265.7142	943.0655
F-stat	1.0072	1.0036	1.0080	1.0042	1.0067	1.0016
p-value	0.8190	0.9073	0.8002	0.8946	0.8309	0.9600
Wishart	32.1781					
p-value	0.0562					

Sd = standard deviation

Table 4. Radiometric calibration statistics. Reference image 021217, target image 010402

5880 training and 2941 test pixels						
Band	intercept	<i>Sd</i>	slope	<i>Sd</i>	R	RMSE
1	21.5470	0.3145	0.6629	0.0040	0.9092	6.2872
2	23.0817	0.1325	0.6585	0.0024	0.9630	3.0348
3	-1.4121	0.1572	1.2402	0.0032	0.9809	1.2350
4	-1.4453	0.1389	1.2408	0.0026	0.9877	1.0942
5	-8.8535	0.1442	1.3420	0.0027	0.9885	1.4860
6	-0.8195	0.0874	1.1016	0.0019	0.9913	2.5593
Means						
Target	75.4771	51.3961	48.3458	53.4872	52.5910	37.5638
Reference	71.4315	56.9330	58.5335	64.9663	61.6960	40.4849
Normalized	71.5790	56.9251	58.5448	64.9215	61.7239	40.5617
t-stat	-1.0744	0.1184	-0.3093	1.3974	-0.6091	-1.0762
p-value	0.2828	0.9063	0.7571	0.1624	0.5425	0.2819
Variances						
Target	669.8285	394.7529	62.5909	81.0594	149.3105	680.8106
Reference	315.7066	177.9897	95.9925	124.6788	268.7566	824.1899
Normalized	294.3261	171.1643	96.2656	124.7971	268.9055	826.2199
F-stat	1.0726	1.0399	1.0028	1.0009	1.0006	1.0025
p-value	0.0573	0.2892	0.9386	0.9795	0.9880	0.9468
Wishart	394.2662					
p-value	0.0000					

Sd = standard deviation

Table 5. Radiometric calibration statistics. Reference image 021217, target image 020115

8989 training and 4495 test pixels						
Band	intercept	Sd	slope	Sd	R	RMSE
1.0000	5.6142	0.3435	0.8158	0.0038	0.9130	6.7397
2.0000	-9.7310	0.4448	0.9637	0.0057	0.8714	6.3519
3.0000	-5.4854	0.2682	0.9358	0.0039	0.9293	3.8207
4.0000	-3.6423	0.2465	0.9450	0.0036	0.9414	3.2090
5.0000	-4.7558	0.2688	0.9541	0.0035	0.9431	3.4717
6.0000	-1.6357	0.1762	0.8335	0.0025	0.9617	5.9594
Means						
Target	85.9030	75.8434	67.0480	67.8331	74.4567	62.0049
Reference	75.7620	63.4525	57.1882	60.5019	66.2545	50.0883
Normalized	75.6972	63.3628	57.2591	60.4631	66.2865	50.0432
t-stat	0.5005	0.6802	-0.9057	0.5977	-0.4527	0.3864
p-value	0.6168	0.4963	0.3651	0.5500	0.6506	0.6991
Variances						
Target	612.2817	341.1624	218.3270	185.6375	219.7061	1129.1055
Reference	431.1311	312.9118	193.8124	167.3529	202.3736	793.6141
Normalized	407.5306	316.8743	191.1996	165.7948	200.0177	784.3486
F-stat	1.0579	1.0127	1.0137	1.0094	1.0118	1.0118
p-value	0.0592	0.6732	0.6492	0.7539	0.6947	0.6939
Wishart	1399.2309					
p-value	0.0000					

Sd = standard deviation

Table 6. Radiometric calibration statistics. Reference image 021217, target image 030424

6248 training and 3125 test pixels						
Band	intercept	<i>Sd</i>	slope	<i>Sd</i>	R	RMSE
1	14.5022	0.3874	0.8684	0.0058	0.8855	6.4012
2	17.0584	0.1521	0.8490	0.0031	0.9615	2.8517
3	-2.7665	0.1510	1.3661	0.0033	0.9819	1.1194
4	-0.6657	0.1044	1.3102	0.0021	0.9922	0.8776
5	-2.7420	0.1006	1.3341	0.0020	0.9930	1.1762
6	-0.5220	0.0529	1.2349	0.0014	0.9962	1.5862
Means						
Target	64.3827	47.3350	44.6608	49.3338	48.4269	30.8730
Reference	70.3763	57.2966	58.1939	64.0176	61.8189	37.6493
Normalized	70.4114	57.2463	58.2443	63.9726	61.8639	37.6038
t-stat	-0.2290	0.7551	-1.5022	1.7494	-1.2690	1.0080
p-value	0.8188	0.4503	0.1331	0.0803	0.2045	0.3135
Variances						
Target	410.9271	254.7837	53.9777	77.7192	152.6103	549.4457
Reference	326.1804	184.8796	99.7735	133.4802	271.8564	837.2445
Normalized	309.8792	183.6524	100.7339	133.4195	271.6159	837.9258
F-stat	1.0526	1.0067	1.0096	1.0005	1.0009	1.0008
p-value	0.1520	0.8524	0.7889	0.9899	0.9803	0.9819
Wishart	533.2684					
p-value	0.00					

Sd = standard deviation

Table 7. Radiometric calibration statistics. Reference image 021217, target image 040808

9051 training and 4526 test pixels						
Band	intercept	<i>Sd</i>	slope	<i>Sd</i>	R	RMSE
1.0000	23.0848	0.1097	1.3027	0.0026	0.9819	2.1793
2.0000	26.5559	0.0914	1.2332	0.0032	0.9716	2.3788
3.0000	30.0141	0.1555	1.2034	0.0067	0.8850	3.3150
4.0000	39.4298	0.1002	0.7943	0.0031	0.9383	2.9361
5.0000	23.4360	0.1688	1.1232	0.0044	0.9358	3.6165
6.0000	2.7676	0.1142	1.5506	0.0036	0.9766	3.0717
Means						
Target	38.9229	25.9532	21.8272	29.9450	35.7225	27.0886
Reference	73.8073	58.6065	56.3358	63.2170	63.5806	44.7872
Normalized	73.7900	58.5618	56.2805	63.2154	63.5589	44.7700
t-stat	0.3183	0.7953	0.7229	0.0282	0.2687	0.2054
p-value	0.7505	0.4266	0.4698	0.9738	0.7881	0.8375
Variances						
Target	203.5076	162.4725	82.0568	178.9890	184.3734	285.5915
Reference	341.3622	244.3351	114.1232	117.3841	229.9487	672.4128
Normalized	345.3628	247.0929	118.8285	112.9289	232.5942	686.6265
F-stat	1.0117	1.0113	1.0412	1.0395	1.0115	1.0211
p-value	0.6952	0.7058	0.1742	0.1932	0.7005	0.4817
Wishart	661.2597					
p-value	0.0000					

Sd = standard deviation

Table 8. Radiometric calibration statistics. Reference image 021217, target image 050320

8392 training and 4196 test pixels						
Band	intercept	<i>Sd</i>	slope	<i>Sd</i>	R	RMSE
1.0000	22.3941	0.1295	0.9135	0.0021	0.9788	2.6868
2.0000	26.4144	0.0821	0.8816	0.0019	0.9809	2.6246
3.0000	30.1120	0.1615	0.8770	0.0052	0.8784	3.6776
4.0000	40.3501	0.0888	0.5698	0.0021	0.9478	2.7261
5.0000	24.0615	0.2074	0.8139	0.0038	0.9177	4.3079
6.0000	0.3284	0.1496	1.1145	0.0033	0.9646	4.8551
Means						
Target	59.0505	38.0605	29.2843	39.1406	51.6208	38.1404
Reference	76.4256	60.0200	55.8098	62.6478	66.0262	42.8372
Normalized	76.3386	59.9671	55.7958	62.6539	66.0754	42.8346
t-stat	1.5631	0.9688	0.1869	-0.1274	-0.5749	0.0238
p-value	0.1181	0.3328	0.8511	0.8993	0.5653	0.9822
Variances						
Target	372.7488	406.5279	126.5101	281.7905	275.1866	604.9279
Reference	311.6753	317.4552	100.3390	96.2788	187.2313	745.5032
Normalized	311.0735	315.9327	97.3131	91.5021	182.2899	751.3448
F-stat	1.0019	1.0048	1.0311	1.0522	1.0271	1.0078
p-value	0.9501	0.8763	0.3214	0.0994	0.3864	0.8005
Wishart	1035.0195					
p-value	0.0000					

Sd = standard deviation

Table 9. Radiometric calibration statistics. Reference image 021217, target image 060727

4000 training and 2000 test pixels						
Band	intercept	<i>Sd</i>	slope	<i>Sd</i>	R	RMSE
1	24.0357	0.2827	1.4709	0.0098	0.9209	4.2068
2	26.9726	0.2908	1.4019	0.0091	0.9252	4.2538
3	23.6314	0.2794	1.3843	0.0092	0.9213	3.9036
4	24.0028	0.2779	1.3520	0.0103	0.9010	4.1530
5	27.9701	0.2612	1.2106	0.0089	0.9069	3.9680
6	18.3105	0.2997	1.4864	0.0098	0.9236	4.1780
Means						
Target	26.0860	29.1535	28.0660	24.7705	27.2260	28.2740
Reference	62.3005	67.8660	62.3955	57.5015	60.9380	60.2230
Normalized	62.4063	67.8415	62.4819	57.4916	60.9288	60.3372
t-stat	-0.6339	0.1493	-0.5918	0.0635	0.0677	-0.6766
p-value	0.5262	0.8814	0.5540	0.9493	0.9457	0.4988
Variances						
Target	166.0296	182.5752	154.7620	141.5596	143.585	171.9259
Reference	335.1678	343.2597	278.1172	244.9755	201.6150	354.6056
Normalized	359.2260	358.7940	296.5495	258.7430	210.4185	379.8549
F-stat	1.0718	1.0453	1.0663	1.0562	1.0437	1.0712
p-value	0.1213	0.3225	0.1515	0.2217	0.3394	0.1242
Wishart	472.8231					
p-value	0.0000					

Sd = standard deviation

Appendix B

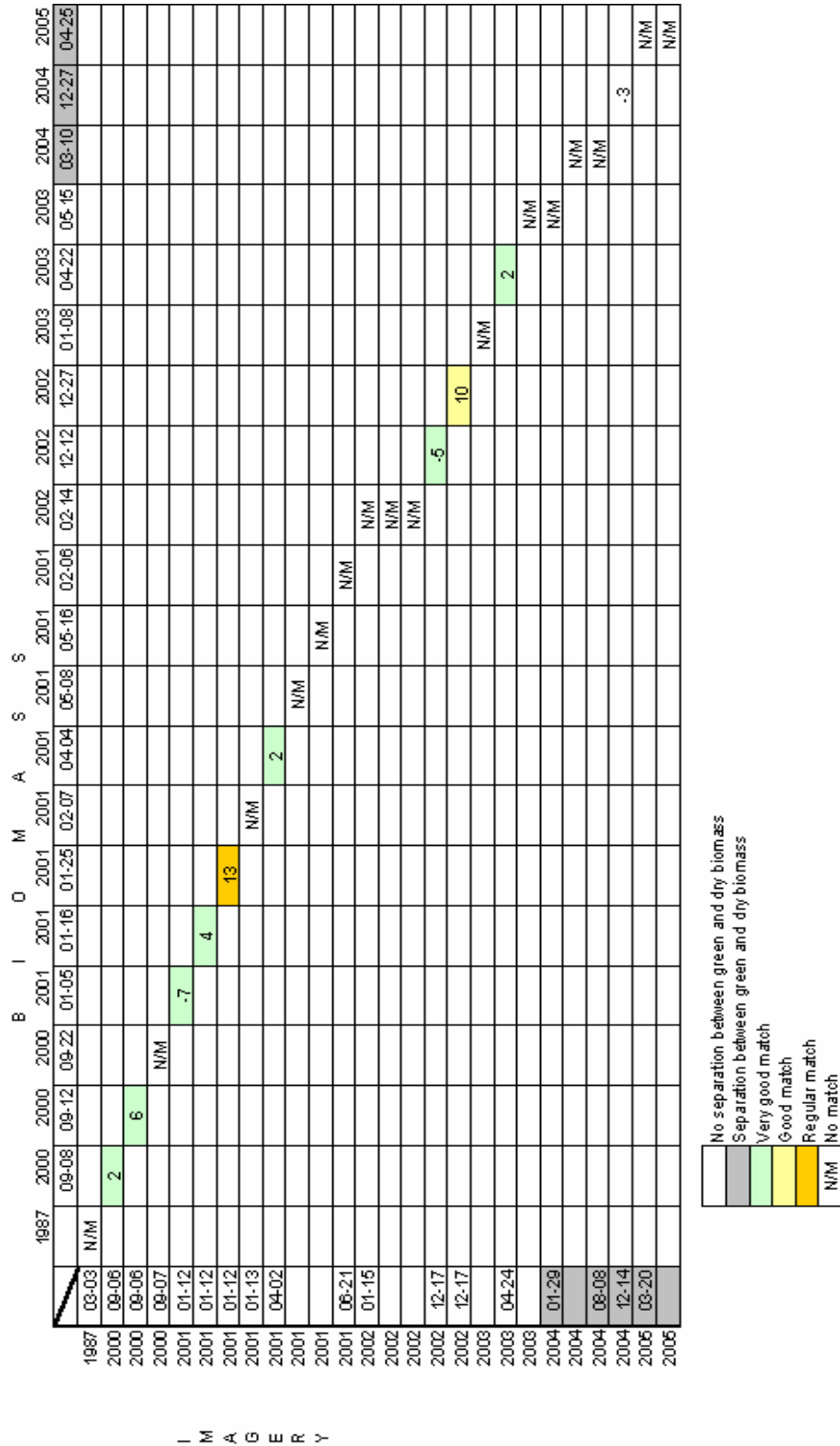


Figure 1. Relationship between available imagery and biomass historical data. The numbers indicate how many days after or before satellite overpasses. Minus (-) indicates that biomass was collected before the satellite overpasses.

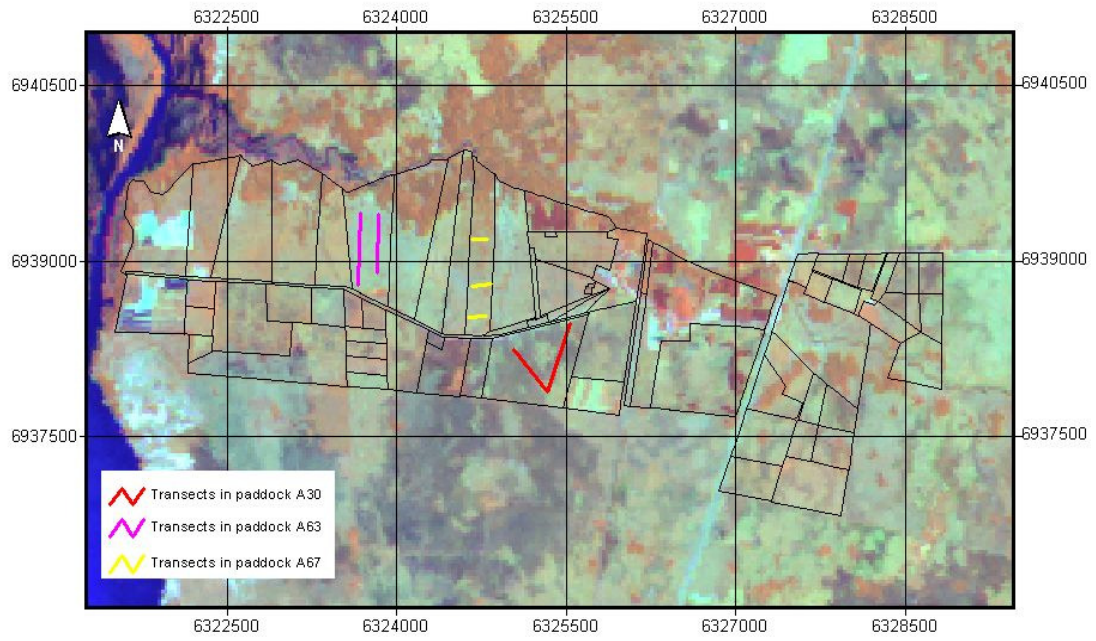


Figure 2. Historical biomass measurements. Map showing the transect location.

Date

Nr.	Vegetation type	Layer	Dominant sp	Management	Soil cover %	Veg. height	erosion	GPS file		Coordinates		others
								x	y	x	y	

Graminoids - **F**orbs
 Shrubs - **T**rees
O =overgrazed
T =traditional
N=not overgrazed
I =intensive
B =recently burned
 wa=water
 wi=wind
 S=sheet
 R=rill
 G=gully

Figure 3. Ground truth evaluation form.

Appendix C

Table 10. Results of testing NDVI calculated from normalised and not normalised cloud free images

	hill	
	<i>normalised</i>	<i>not normalised</i>
mean	0.27	0.44
variance	0.0001	0.0004
observations	45	45
pearson correlation	0.97	
hypothesized mean difference	0	
df	44	
t stat	-112.45	
p(t<=t) one-tail	0.00	
t critical one-tail	1.68	
p(t<=t) two-tail	0.00	0.05
t critical two-tail	2.02	

Not significantly different

Historical non cloudy images

NRN = NDVI calculated from not radiometrically normalised images.

RN = NDVI calculated from radiometrically normalised images.

Table 11. Results of testing NDVI calculated from a normalised and not normalised cloudy image

	plain	
	<i>normalised</i>	<i>not normalised</i>
mean	0.22	0.37
variance	0.0004	0.0008
observations	45	45
pearson correlation	0.95	
hypothesized mean difference	0	
df	44	
t stat	-84.16	
p(t<=t) one-tail	0.00	
t critical one-tail	1.68	
p(t<=t) two-tail	0.00	0.05
t critical two-tail	2.02	

Significantly different

Not normalised = NDVI calculated from not radiometrically normalised images.

Normalised = NDVI calculated from radiometrically normalised images.

Table 12. Results of testing grassland total biomass on plains and on hills

	total biomass (kg ha ⁻¹)	
	<i>plain</i>	<i>hill</i>
mean	2271.57	3496.84
variance	1225563.41	1102531.37
observations	10	9
pooled variance	1167666.0	
df	17	
t stat	-2.47	
p(t<=t) one-tail	0.01	
t critical one-tail	1.74	
p(t<=t) two-tail	0.02	0.05
t critical two-tail	2.11	

sites have significantly different total biomass (kg ha⁻¹)

Table 13. Results of testing grassland percentage of SDM on plains and on hills

	standing dead material (%)	
	<i>plain</i>	<i>hill</i>
mean	38.85	24.33
variance	37.23	31.00
observations	10	9
pooled variance	34.30	
df	17	
t stat	5.40	
p(t<=t) one-tail	0.00	
t critical one-tail	1.74	
p(t<=t) two-tail	0.00	0.05
t critical two-tail	2.11	

sites have significantly different % of SDM

Table 14. Results of testing INTECO values between plains and hills

	INTECO	
	<i>plain</i>	<i>hill</i>
mean	34.44	24.34
variance	8.94	37.40
observations	10	9
pooled variance	22.33	
df	17	
t stat	4.65	
p(t<=t) one-tail	0.00	
t critical one-tail	1.74	
p(t<=t) two-tail	0.00	0.05
t critical two-tail	2.11	

sites have significantly different INTECO

Table 15. Results of testing grassland percentage of BS on plains and on hills

	bare soil (%)	
	<i>plain</i>	<i>hill</i>
mean	19.88	22.78
variance	33.05	21.44
observations	10	9
pooled variance	27.59	
df	17	
t stat	-1.20	
p(t<=t) one-tail	0.12	
t critical one-tail	1.74	
p(t<=t) two-tail	0.25	0.05
t critical two-tail	2.11	

sites have no significantly different % of bare soil

Table 16. Results of testing grassland percentage of M on plains and on hills

	mulch (%)	
	<i>plain</i>	<i>hill</i>
mean	13.50	12.00
variance	50.81	31.00
observations	10	9
pooled variance	41.49	
df	17	
t stat	0.51	
p(t<=t) one-tail	0.31	
t critical one-tail	1.74	
p(t<=t) two-tail	0.62	0.05
t critical two-tail	2.11	

sites have no significantly different % of mulch

Table 17. Results of testing grassland NDVI values between plains and hills

	NDVI	
	<i>plain</i>	<i>hill</i>
mean	0.22	0.27
variance	0.00	0.00
observations	10	9
pooled variance	0.00	
df	17	
t stat	-6.15	
p(t<=t) one-tail	0.00	
t critical one-tail	1.74	
p(t<=t) two-tail	0.00	0.05
t critical two-tail	2.11	

sites have significantly different NDVI

Table 18. Results of testing grasses protein concentration between plains and hills

	protein (%)	
	<i>plain</i>	<i>hill</i>
mean	7.3	7.03
variance	0.070	0.74
observations	10	9
pooled variance	0.38	
hypothesized mean difference	0	
df	17	
t stat	0.97	
p(t<=t) one-tail	0.17	
t critical one-tail	1.74	
p(t<=t) two-tail	0.34	0.05
t critical two-tail	2.11	

no significant difference between sites

Table 19. Results of testing grasses nitrogen concentration between plains and hills

	nitrogen (%)	
	<i>plain</i>	<i>hill</i>
mean	1.17	1.12
variance	0.00	0.02
observations	10	9
pooled variance	0.01	
hypothesized mean difference	0	
df	17	
t stat	0.97	
p(t<=t) one-tail	0.17	
t critical one-tail	1.74	
p(t<=t) two-tail	0.34	0.05
t critical two-tail	2.11	

no significant difference between sites

Table 20. Results of testing grasses carbon concentration between plains and hills

	carbon (%)	
	<i>plain</i>	<i>hill</i>
mean	43.78	43.11
variance	0.11	0.17
observations	10	9
pooled variance	0.14	
hypothesized mean difference	0	
df	17	
t stat	33664,00	
p(t<=t) one-tail	0.00	
t critical one-tail	1.74	
p(t<=t) two-tail	0.34	0.05
t critical two-tail	2.11	

significant difference between sites

Table 21. Results of testing interpolated and not interpolated biomass means

	<i>no interpolated</i>	<i>interpolated</i>
mean	2789.56	2700.97
variance	2145133.03	981682.01
observations	25	32
pooled variance	1489369.73	
hypothesized mean difference	0	
df	55	
t stat	0.27	
p(t<=t) one-tail	0.39	
t critical one-tail	1.67	
p(t<=t) two-tail	0.79	0.05
t critical two-tail	2.00	

No significant difference between ground measurements and interpolated data.

Appendix D

Table 22. Floristic composition on the hill site

species	total (%)
<i>Vernonia chamaedrys</i> Lees.	34.58
<i>Sorghastrum agrostoides</i> (Speg.) Hitchc.	18.38
<i>Paspalum notatum</i> Flügge	12.57
<i>Sorghastrum nutans</i> (L.) Nash	11.53
<i>Eryngium horridum</i> Malme	6.75
<i>Heimia salicifolia</i> (H. B. K.) Link	4.99
<i>Paspalum plicatulum</i> Michx.	1.62
<i>Aristida leptochaeta</i> Hackel	1.56
<i>Axonopus affinis</i> Chase	0.73
<i>Andropogon selloanus</i> (Hack.) Hackel	0.66
<i>Desmodium incanum</i> Dc.	0.65
<i>Sida rhombifolia</i> L.	0.63
<i>Sida urens</i> L.	0.63
<i>Cyperus entrerrianus</i> Bcklr.	0.6
<i>Leersia hexandra</i> Swartz	0.57
<i>Piptochaetium montevidense</i> (Spreng.) Parodi	0.57
<i>Panicum milioides</i> Nees.	0.52
<i>Eupatorium ivaefolium</i> L.	0.47
<i>Aspilia montevidensis</i> (Spreng.) Ok.	0.36
<i>Tridens brasiliensis</i> (Nees ex Steudel)	0.23
<i>Paspalum simplex</i> Morong.	0.19
Sp.	0.19
* <i>Aeschynomene falcata</i> (Poir.) Dc.	0.19
<i>Orthoppapus angustifolius</i> (Sw.) Gleason	0.13
<i>Gymnopogon biflorus</i> R. Pilger	0.1
<i>Chloris distichophylla</i> M. Lagasca	0.1
<i>Eupatorium christieanum</i> Baker	0.06
<i>Verbena rigida</i> Spr.	0.06
<i>Schizachyrium paniculatum</i> (Kunth) Herter	0.06
<i>Eragrostis lugens</i> Nees	0.06
<i>Sida tuberculata</i> R. E. Fries	0.06
<i>Dichondra repens</i> Forst	0.06
<i>Sida spinosa</i> L.	0.06
<i>Carex sororia</i> Kunth	0.06
<i>Eryngium elegans</i> Cham. et Schlecht.	
<i>Setaria geniculata</i> (Lam.) Pal. de Beauvois	
<i>Turnera ulmitolia</i> L.	
<i>Euphorbia selloi</i> (Kl. et Garke) Boiss	
<i>Sisyrinchium</i> L.	
<i>Desmanthus depressus</i> H. et B.	
<i>Plantago australis</i> Lam.	
<i>Cyperus obtusatus</i> (Presl.) Mattf. et Kuek.	
<i>Desmanthus virgatus</i> (L.) Wild.	
<i>Paspalum alnum</i> Chase	
<i>Rhynchosia minima</i> (L.) DC	
<i>Eragrostis bahiensis</i> (Schr. ex Schult) Schult	
<i>Fimbristylis dichotoma</i> (L.) Vahl.	
<i>Aristida venustula</i> Arechav.	
<i>Cyperus sesquiflorus</i> (Torr.) Mattf. et Kuek.	
<i>Sporobolus indicus</i> (L.) R. Brown	
<i>Stachytarpheta cayannensis</i> (L. C. Rich.) Vahl	
<i>Rhynchospora tenuis</i> Link	

* the name of this species was not known.

Table 23. Floristic composition on the plain site

species	total (%)
<i>Paspalum intermedium</i> Munro ex Morong et Britton	44.4
<i>Andropogon lateralis</i> Nees	20.65
<i>Sorghastrum agrostoides</i> (Speg.) Hitchc.	16.56
<i>Axonopus affinis</i> Chase	9.14
<i>Paspalum urvillei</i> Steud.	2.22
<i>Panicum dichotomiflorum</i> Michx.	1.56
<i>Paspalum plicatulum</i> Michx.	0.95
<i>Panicum laxum</i> O. Schwartz	0.82
<i>Schizachyrium paniculatum</i>	0.63
<i>Eleocharis viridans</i> Kük. ex Osten	0.48
<i>Rhynchospora scutellata</i> Griseb.	0.47
<i>Rhynchospora corymbosa</i> (L.) Britt.	0.47
<i>Panicum milioides</i> Nees	0.36
<i>Eleocharis nodulosa</i> (Roth.) Schult.	0.19
<i>Leersia hexandra</i> Swartz	0.19
<i>Bouteloua megapotamica</i> (Spreng.) O. Kuntze	0.19
<i>Aster squamatus</i> (Spreng.) Hieron.	0.16
<i>Cyperus entrerrianus</i> Bcklr.	0.1
<i>Eupatorium candolleanum</i> H. et B.	0.1
<i>Paspalum ionanthum</i> Chase	0.1
<i>Sporobolus indicus</i> (L.) R. Brown	0.1
<i>Setaria gracilis</i> H. B.K.	0.1
<i>Eragrostis bahiensis</i> (Schrad. ex Schult) Schult	0.06
<i>Rhynchospora barrosiana</i> Gua.	
<i>Eryngium ebracteatum</i> Lam.	
<i>Hyptis lappacea</i> Bentham	
<i>Rhynchospora tenuis</i> Link	
<i>Conyza bonariensis</i> (L.) Cronq.	
<i>Hyptis</i> Jacq.	
<i>Eragrostis airoides</i> Nees	
<i>Scutellaria racemosa</i> Persoon	
<i>Asclepias mellodora</i> St-Hil.	
<i>Eclipta prostrata</i> (L.) L.	
<i>Alternanthera philoxeroides</i> (Mart.) Griseb.	
<i>Phyllanthus lathyroides</i> Kunth.	
<i>Luziola leiocarpa</i> Lidman	
<i>Ludwigia</i> L.	
<i>Picrocia longifolia</i> D. Don	
<i>Oxalis</i> L.	
<i>Polygonum punctatum</i> Elliot	
<i>Pterocaulom polystachyum</i> DC	
<i>Cyperus cayennensis</i> (Lam.) Britt.	
<i>Sida rhombifolia</i> L.	
<i>Chaptalia</i> Vent.	
<i>Habenaria</i> Willd.	
<i>Setaria geniculata</i> (Lam.) Pal. de Beauvois	
<i>Baccharis notorsegila</i> Griseb.	

Table 24. Species biomass share on the hill site

species	dry matter (kg)	%
<i>Vernonia chamaedrys</i>	1775.82	50.66
<i>Sorghastrum agrostoides</i>	479.16	13.67
<i>Eryngium horridum</i>	396.47	11.3
<i>Sorghastrum nutans</i>	381.44	10.9
<i>Paspalum notatum</i>	130.09	3.7
<i>Heymia salicifolia</i>	63.49	1.8
<i>Aristida leptochaeta</i>	53.03	1.5
<i>Axonopus affinis</i>	45.71	1.3
<i>Paspalum plicatulum</i>	43.24	1.2
<i>Andropogon selloanus</i>	29.58	0.84
* Sp.	13.81	0.39
<i>Sida rhombifolia</i>	11.3	0.32
<i>Aeschynomene falcata</i>	10.9	0.31
<i>Leersia hexandra</i>	8.6	0.25
<i>Desmodium incanum</i>	7.5	0.22
<i>Aspilia montevidensis</i>	7.4	0.21
<i>Piptochaetium montevidense</i>	7.2	0.21
<i>Cyperus entrerrianus</i>	6.3	0.18
<i>Eupatorium ivaefolium</i>	5.4	0.15
<i>Tridens brasiliensis</i>	5.0	0.14
<i>Panicum milioides</i>	4.3	0.12
<i>Gymnopogon biflorus</i>	4.0	0.11
<i>Orthoppapus angustifolius</i>	3.9	0.11
<i>Schizachyrium paniculatum</i>	3.3	0.09
<i>Sida urens</i>	3.3	0.09
<i>Sida tuberculata</i>	1.1	0.03
<i>Paspalum simplex</i>	0.77	0.02
<i>Verbena rigida</i>	0.62	0.02
<i>Eupatorium christeanum</i>	0.57	0.02
<i>Eragrostis lungens</i>	0.49	0.01
<i>Dichondra repens</i>	0.49	0.01
<i>Sida spinosa</i>	0.49	0.01
<i>Carex sororia</i>	0.46	0.01
<i>Chloris distichophylla</i>	0.35	0.01
<i>Eryngium elegans</i>		
<i>Setaria geniculata</i>		
<i>Turnera ulmifolia</i>		
<i>Euphorbia selloi</i>		
<i>Sisyrinchium sp.</i>		
<i>Desmanthus depressus</i>		
<i>Plantago australis</i>		
<i>Cyperus obtusatus</i>		
<i>Desmanthus virgatus</i>		
<i>Paspalum alium</i>		
<i>Rhynchosia minima</i>		
<i>Eragrostis bahiensis</i>		
<i>Fimbristylis dichotoma</i>		
<i>Aristida venustula</i>		
<i>Cyperus sesquiflorus</i>		
<i>Sporobolus indicus</i>		
<i>Stachytarpheta cayannensis</i>		
<i>Rhynchospora tenuis</i>		

* the name of one species was not known.

Table 25. Species biomass share on the plain site

species	dry matter (kg)	%
<i>Paspalum intermedium</i>	1037.5	45.36
<i>Sorghastrum agrostoides</i>	611.44	26.73
<i>Andropogon lateralis</i>	418.79	18.31
<i>Axonopus affinis</i>	56.2	2.5
<i>Paspalum urvillei</i>	38.8	1.7
<i>Paspalum plicatulum</i>	34.8	1.5
<i>Rhynchospora corymbosa</i>	21.73	0.95
<i>Schizachyrium paniculatum</i>	19.61	0.86
<i>Paspalum ionanthum</i>	8.3	0.36
<i>Eleocharis viridans</i>	7.8	0.34
<i>Eleocharis nodulosa</i>	6.0	0.26
<i>Panicum laxum</i>	5.0	0.22
<i>Cyperus entrerrianus</i>	4.8	0.21
<i>Setaria gracilis</i>	4.5	0.19
<i>Leersia hexandra</i>	4.1	0.18
<i>Rhynchospora scutellata</i>	3.6	0.16
<i>Panicum milioides</i>	1.8	0.08
<i>Panicum dichotomiflorum</i>	1.2	0.05
<i>Sporobolus indicus</i>	0.43	0.02
<i>Bouteloua megapotamica</i>	0.39	0.02
<i>Aster squamatus</i>	0.21	0.01
<i>Eragrostis bahiensis</i>	0.13	0.01
<i>Eupatorium candolleanum</i>	0.08	
<i>Rhynchospora barrosiana</i>		
<i>Eryngium ebracteatum</i>		
<i>Hyptis lappacea</i>		
<i>Rhynchospora tenuis</i>		
<i>Conyza bonariensis</i>		
<i>Hyptis sp.</i>		
<i>Eragrostis airoides</i>		
<i>Scutellaria racemosa</i>		
<i>Asclepia mellodora</i>		
<i>Eclipta prostrata</i>		
<i>Alternanthera philoxeroides</i>		
<i>Phyllanthus lathyroides</i>		
<i>Luziola leiocarpa</i>		
<i>Ludwigia sp.</i>		
<i>Picrocia longifolia</i>		
<i>Oxalis sp.</i>		
<i>Polygonum punctatum</i>		
<i>Pterocaulom polystachyum</i>		
<i>Cyperus cayennensis</i>		
<i>Sida rhombifolia</i>		
<i>Chaptalia sp.</i>		
<i>Habenaria</i>		
<i>Setaria geniculata</i>		
<i>Baccharis notorsegila</i>		

Appendix E

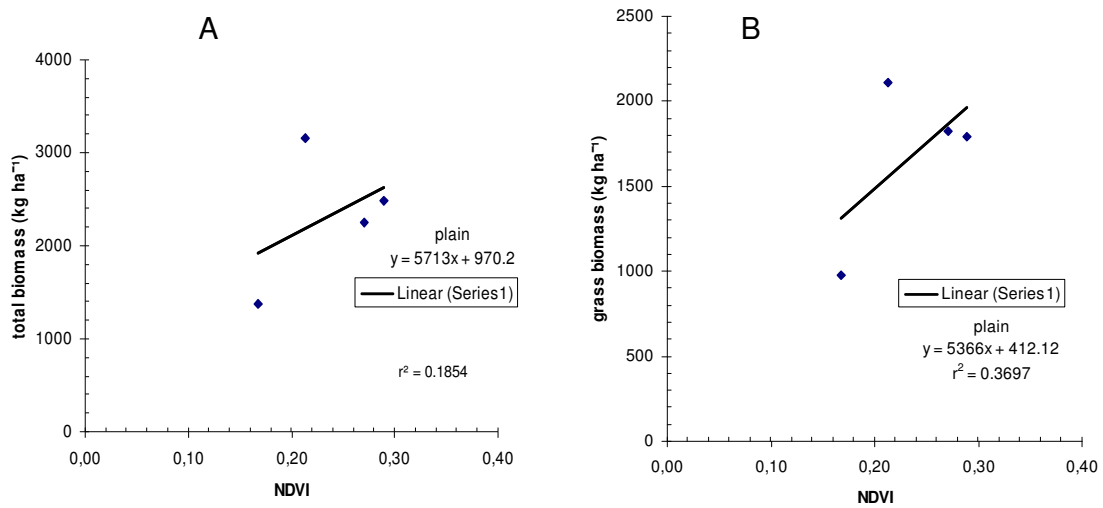


Figure 4. Relationship between historical total biomass (A) and grasses (B), in the plain area and NDVI.

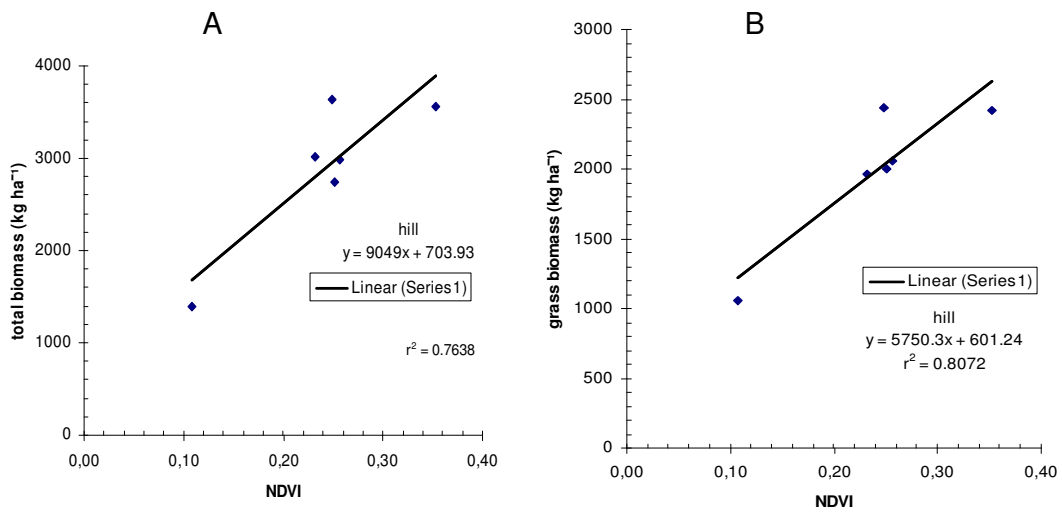


Figure 5. Relationship between historical total biomass (A) and grasses (B), in the hill area and NDVI.

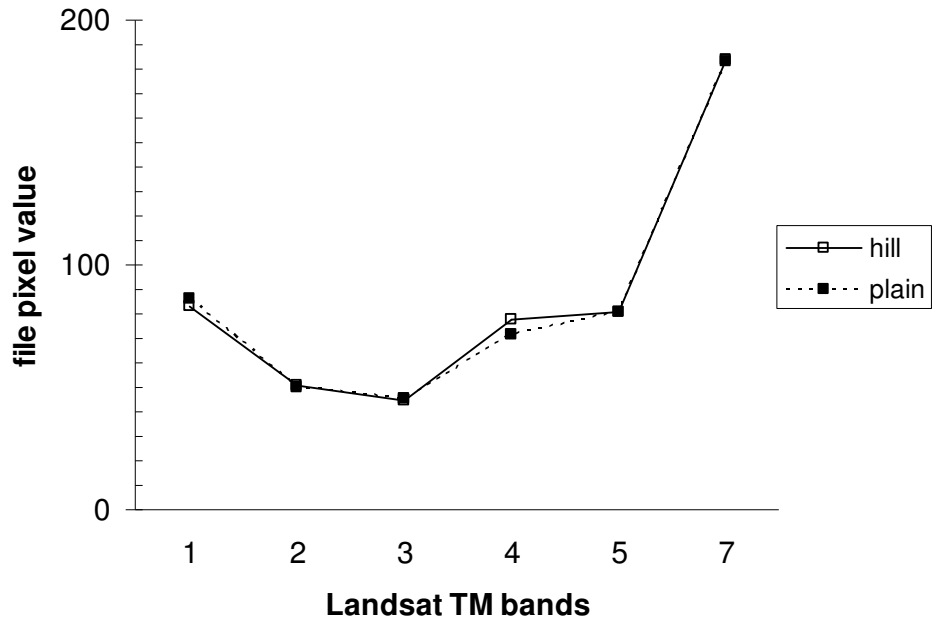


Figure 6. Mean file pixel value for each TM band on hills and plains.

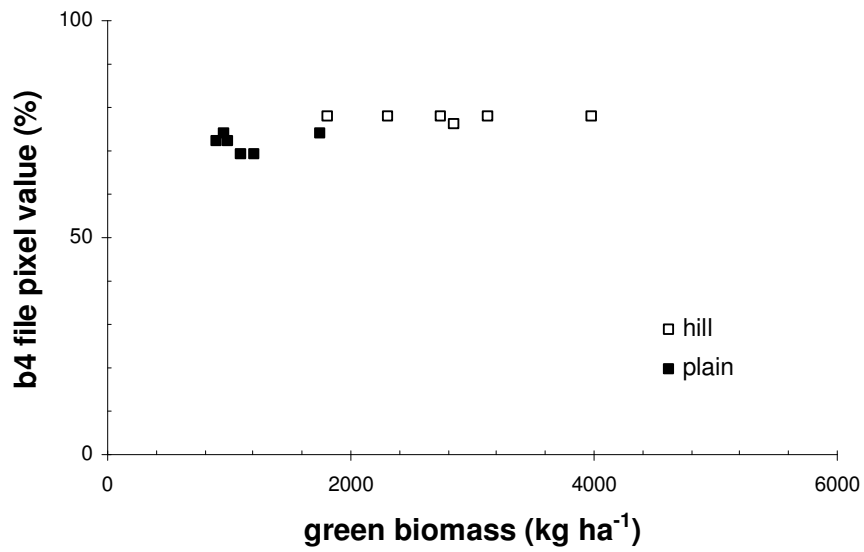


Figure 7. Relationship of mean file pixel value for band 4 and green biomass.

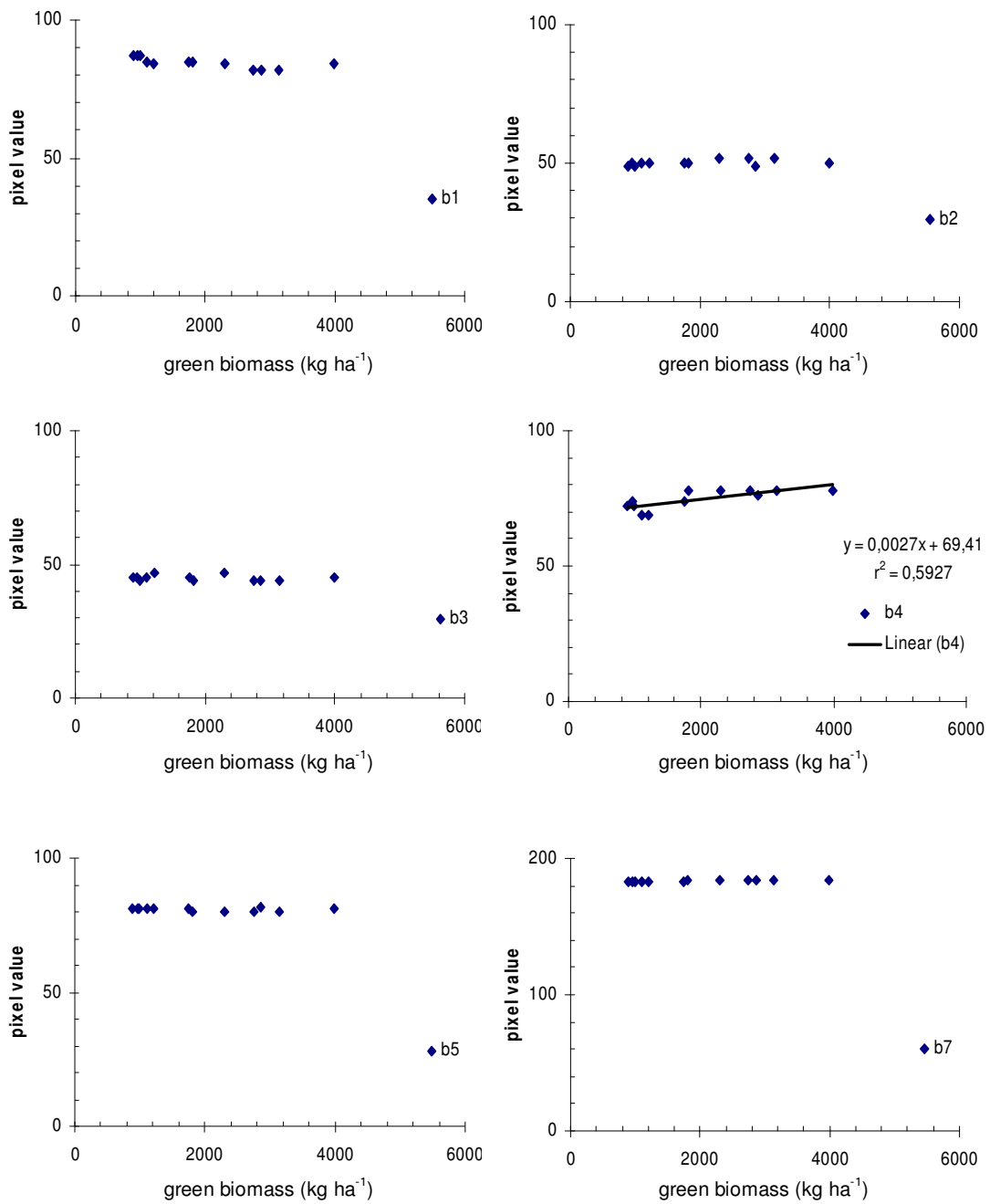


Figure 8. Relationship between interpolate green biomass and file pixel value for each Landsat band (except band 6), b1 to b7 stands for band 1 to band 7.

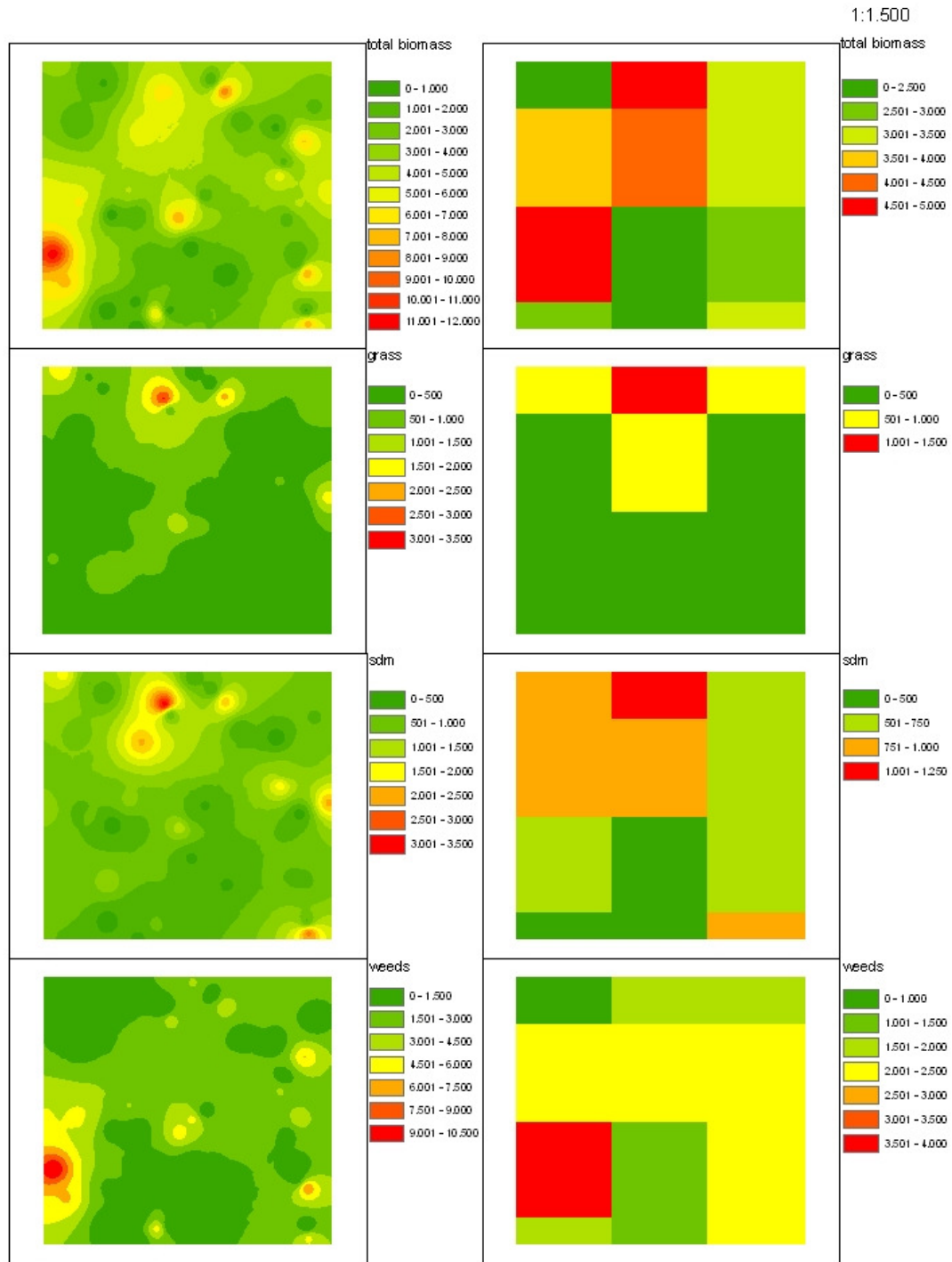


Figure 9. Hill grassland variability indicated by IDW interpolated point biomass values (left) and Landsat pixel size interpolated biomass values (right).

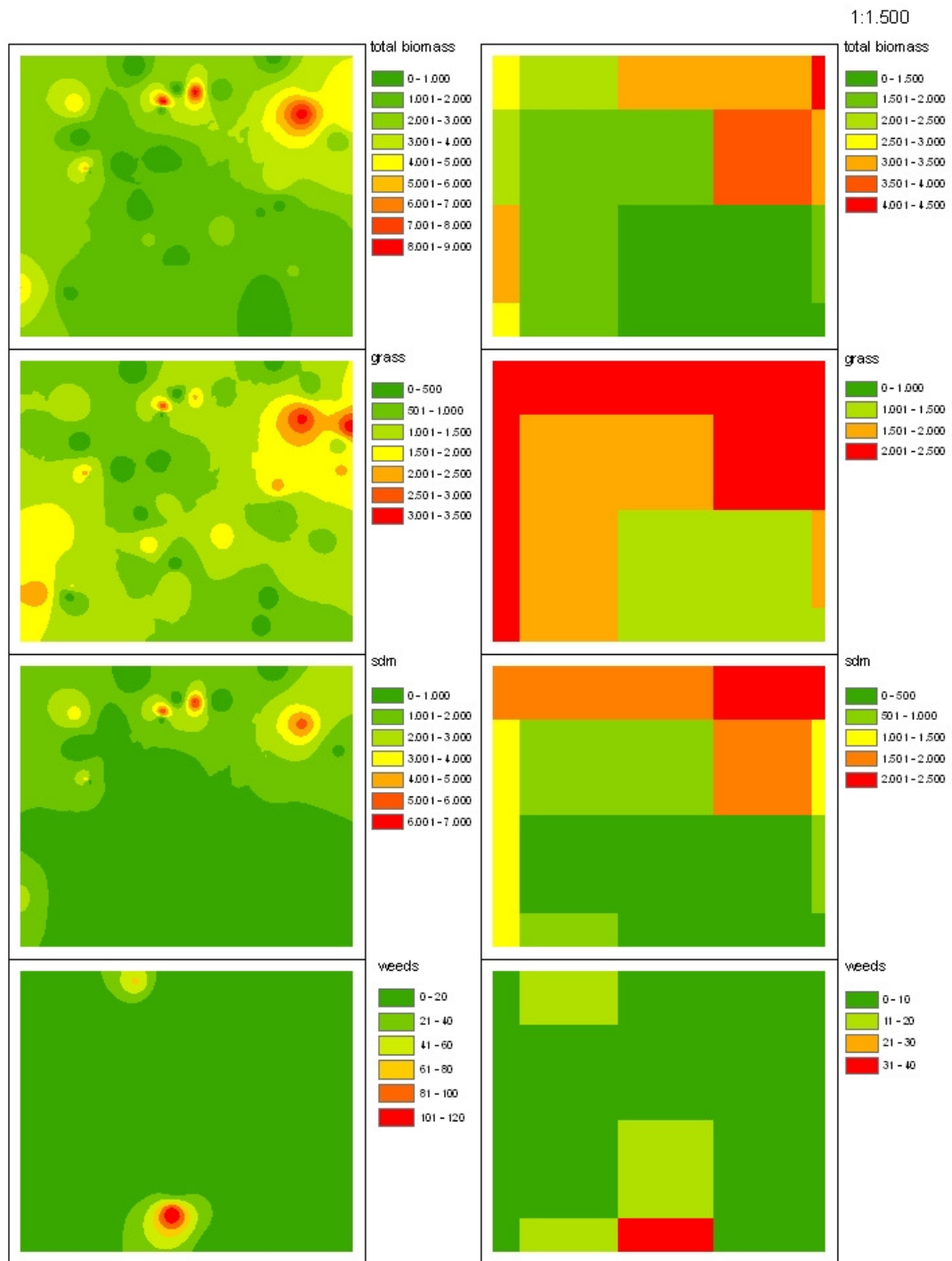


Figure 10. Plain grassland variability indicated by IDW interpolated point biomass values (left) and Landsat pixel size interpolated biomass values (right).

Appendix F

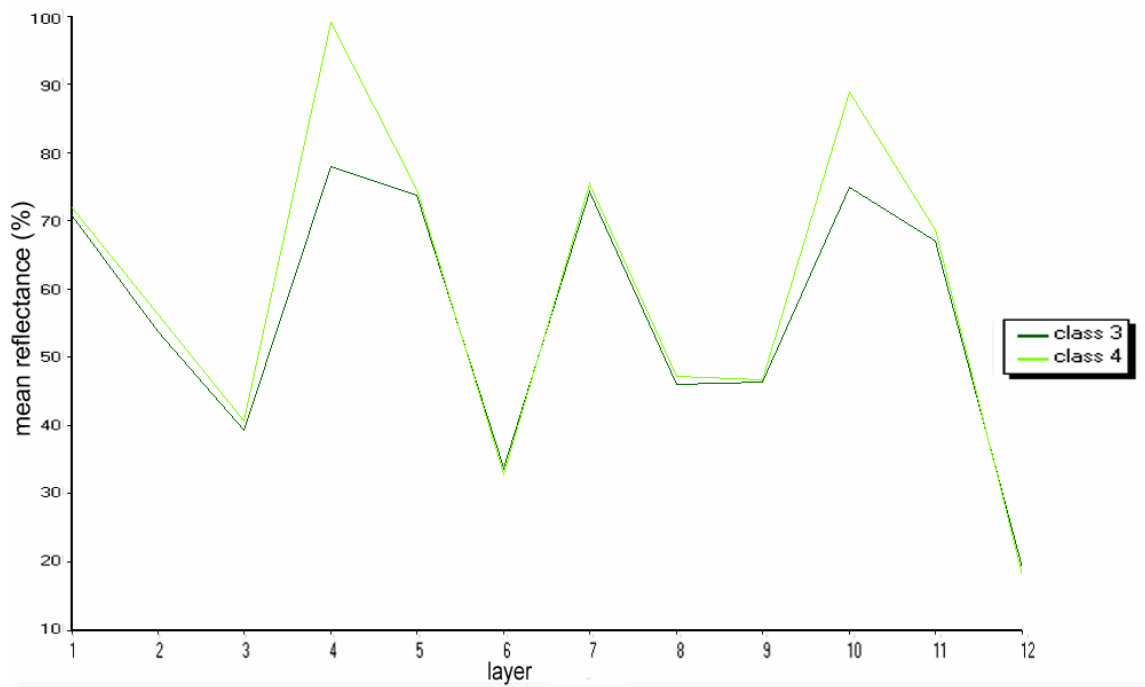


Figure 11. Reflectance of classes 3 and 4 taken from training areas for supervised classification. The first six layers corresponded to year 2002 whilst the last 6 to year 2005.

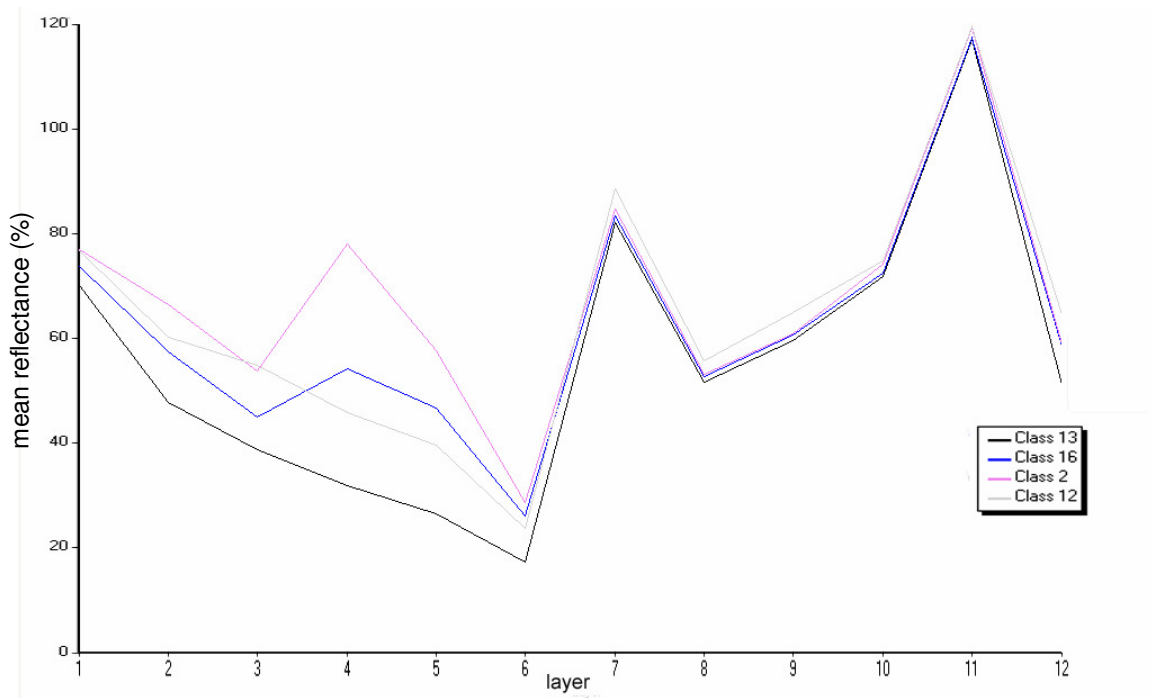


Figure 12. Reflectance of classes 2, 12, 13 and 16 taken from training areas for supervised classification. The first six layers corresponded to year 2002 whilst the last six to year 2005.

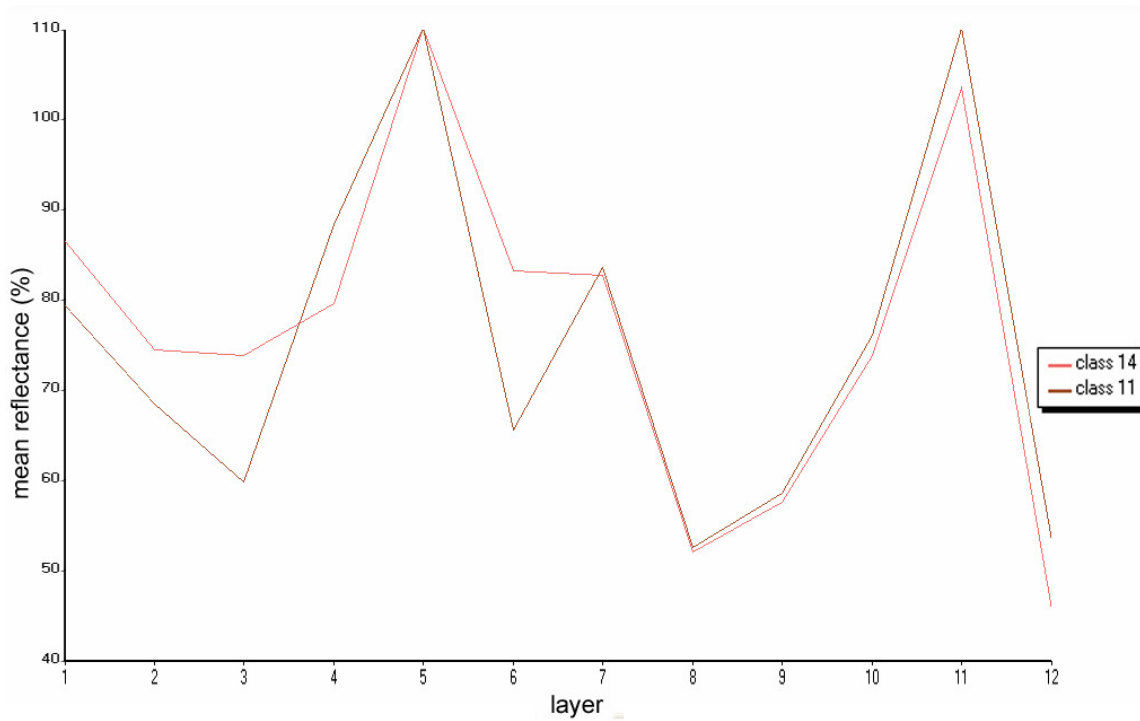


Figure 13. Reflectance of classes 11 and 14 taken from training areas for supervised classification. The first six layers corresponded to year 2002 whilst the last six to year 2005.

Appendix G

Table 26. Equivalence between livestock categories and animal units (A. U.) system*

categorie unit	equivalence
bull	1.3 A. U. Average during 1 year.
cow	1 A. U. Average during 1 year or
average cow	1.4 A. U. From labor to wean (6 months) y 0.6 A. U. from wean to labor (6 months).
calf / veal	0.6 A. U. From wean to 1 year old.
castrated calf (A)	0.7 A. U. From 1 to 2 years old.
castrated calf (B)	0.8 A. U. From 2 years old or more than 300 kg.
castrated calf (fat)	1 A. U. From 400 kg till sale.
young cow (A)	0.7 A. U. From 1 to 2 years old.
young cow (B)	0.8 A. U. From 2 years old or more than 300 kg or pregnant.

* Adapted from [CARRILLO, J. 2001](#)

Table 27. Grassland resource availability for each class

class	grassland resource (%)
1	100
2	100
3	30
4	30
5	100
6	100
7	100
8	100
9	100
10	100
11	100
12	100
13	100
14	50
15	30
16	100
17	100
18	100
19	-
20	-
21	-
22	-
23	-
24	50
25	50
26	-

APPENDIX H

Table 28. Accuracy assessment of the combined 26-class classification

class	reference totals	classified totals	classified correctly	producers accuracy	users accuracy	kappa coefficient
1	2	3	2	100.0	66.7	0.6662
2	21	20	17	80.9	85.0	0.8477
3	91	90	74	81.3	82.2	0.8097
4	30	35	28	93.3	80.0	0.7956
5	110	94	74	67.3	78.7	0.7689
6	285	286	245	86.0	85.7	0.8195
7	58	51	47	81.0	92.2	0.9181
8	41	37	33	80.5	89.2	0.8886
9	13	10	9	69.2	90.0	0.8991
10	43	48	36	83.7	75.0	0.7420
11	161	169	123	76.4	72.8	0.6920
12	171	146	125	73.1	85.6	0.8359
13	17	15	14	82.3	93.3	0.9325
14	18	12	11	61.1	91.7	0.9156
15	97	104	60	61.9	57.7	0.5451
16	40	39	36	90.0	92.3	0.9208
17	69	108	54	78.3	50.0	0.4738
18	12	9	7	58.3	77.8	0.7758
19	3	2	2	66.7	100.0	10.000
20	7	11	3	42.9	27.3	0.2690
21	0	0	0	-	-	0.0000
22	17	17	9	52.9	52.9	0.5236
23	1	1	1	100.0	100.0	10.000
24	1	1	1	100.0	100.0	10.000
25	0	0	0	-	-	0.0000
26	77	77	77	100.0	100.0	10.000
totals	1385	1385	1088			

Overall classification accuracy = 78.56%

Overall kappa statistics = 0.7625

Table 29. Confusion matrix for the 8-class grazing pressure / grazing intensity level classification

classified data	reference data								total	users accuracy (%)
	1	2	3	4	5	6	7	8		
1	56	16	3	1	2	3		3	84	66.7
2		62	2		1			2	67	80.5
3	10	1	25						36	96.1
4	2		2	6		2	2		14	40.0
5		1			27	3			31	87.1
6		3				13			16	81.2
7							12		12	100.0
8								8	8	100.0
total	68	83	32	7	30	21	14	13	268	
producers accuracy (%)	82.3	74.7	78.1	85.7	90.0	61.9	85.7	40.0		

Overall Classification Accuracy = 77.36%

Overall Kappa Statistics = 0.7146

Appendix I

Class 1, pastures. Vegetation characterized by non native, summer growing grasses, mainly *Brachiaria* and *Setaria* species (palatable species). Pastures normally are sown in hills with good soils and were properly managed.

Class 2, marsh (2). Palatable semi-waterlogged vegetation located close to the Paraná riverside and its islands, usually affected by floods. The dominating tall grass species are *Panicum grumosum* and *P. rivulare*.

Class 3, close forest. Semi-evergreen vegetation represented by trees, normally located on hills. Soil coverage is higher than 70%.

Class 4, close forest (2). Broad leaf evergreen vegetation represented by trees located in the Paraná riverside and on its islands. This class is characterized by a high biodiversity level and a high percentage of soil coverage, more than 70%.

Class 5, grassland not overgrazed (on hills). Vegetation dominated by tall close grasses and very sparse woody and herbaceous shrubs. Dominating species are *Andropogon lateralis* and *Sorghastrum agrostoides* (palatable when very young, limited palatability when dry).

Class 6, grassland not overgrazed (on plains). The vegetation is characterized by perennial tall grasses. Dominant species are *A. lateralis* and *S. agrostoides* which form close swards. An interesting “reticular” erosion pattern characterizes this very plain area. It is often very difficult to walk (fig. 1). Productive, fast growing grasses thanks to a water layer which stays for around five months every year, but grasses lose quality quickly.

Class 7, grassland burned 2002 (on plains). The current dominant vegetation is the same as in class 6, but was identified as burned on the image of 2002.

Class 8, grassland burned 2005 (on plains). The current dominant vegetation is the same as in class 6, but was identified as burned on the image of 2005.

Class 9, grassland burned 2005 (on hills). The current dominant vegetation is the same as in class 5, but was identified as burned on the image.

Class 10, grassland burned both dates (on plains). The dominant vegetation is the same as in class 6. This area is simultaneously identified as burned on both images.

Class 11, short grasses - intensively grazed (on hills). Vegetation dominated

by short grasses and herbaceous shrubs like *Vernonia chamaedrys* and *Baccharis coridifolia* (not palatable weeds, the latter toxic). Dominant species are *Paspalum notatum* (palatable), *A. lateralis* and *Axonopus* species (highly palatable).

Class 12, grassland intensively grazed (on plains). Areas were even though the vegetation is similar to that in class 6, the higher grazing pressure over long time helped to increase the proportion of short and more palatable species, like *P. notatum* and *Axonopus* species ([Carnevali 1994](#)).

Class 13, short grasses - intensively grazed (on plains). Dominant vegetation includes *Eleocharis* (medium-low palatability) and palatable species of *Axonopus*, *Paspalum* and *Luziola*. Overgrazing features during winter and / or dry seasons were registered here during the field campaign.

Class 14, fallow. Represented by sparse vegetation and variable percentages of BS, depending on the length of the fallow period. Even though semi-natural vegetation slowly regenerates after a cropping period, previous status is normally not recovered fully.

Class 15, open forest. Different forest types sharing some common characteristics, all present sparse trees, all are located in plain areas and more or less affected by soil sodicity. Local names are given to the forest according to the dominant species. Forests of *Prosopis nigra* and *P. alba* (deciduous trees), forests of *Aspidorperma quebracho blanco* and forests of *Schinopsis balansae* (which was intensively logged in the past) or mixed forest. Overgrazing and sheet erosion features are easily detected on this area. Soil coverage ranges from 10 to 50%. To make the map more reliable these forest types were collapsed on one class, so less information is displayed on the map, but the remaining information is more reliable ([Congalton et al. 1999](#)). Therefore, open forest includes heterogeneous forests that were collapsed, with the help of soil data, in one single class.

Class 16, marsh (3). Semi permanent waterlogged areas intensively grazed in wet periods which are showing strong overgrazing, mainly during dry periods. Dominant vegetation includes *Eleocharis* and *Luziola* species.

Class 17, not vegetated. This class includes towns, roads and all other naturally bare soil areas like those affected by sheet erosion and sand depositions by the river and creeks. All these areas are spectrally very similar.

The common feature is the high reflectance in the visible region but low in NIR region. On the surface there is normally no vegetation or it is very sparse.

Class 18, erosion. Not vegetated areas severely affected by gully erosion. Located in the Paraná riverside where deep slopes and soil type increases the erosion risks.

Class 19, perennial (orchards and plantations). Rain fed tree crops, citrus and plantations, pine and eucalyptus are included here.

Class 20, marsh (1). Permanently waterlogged areas with organic soils, medium deep water layer and herbaceous plants, rooted forbs, typhas, tall grass like species and also floating vegetation (mostly all are non palatable species).

Class 21, water reservoir. Artificial permanent to semi-permanent shallow water bodies (2-3 meters deep).

Class 22, waterlogged grassland. The vegetation is represented by perennial tall grasses. Dominant species is *Panicum prionitis* (non palatable).

Class 23, lagoon. Natural permanent to semi-permanent shallow water bodies (2-5 meters deep). Vegetation grows neither on the surface, nor on the bottom.

Class 24, rice. Single irrigated crop with homogeneous cover. The cropping period is during summer, lasting three to four years, and with six months of winter fallow every year. After a cropping cycle finishes the field is normally leaved for longer fallow period. Fields are often grazed during fallow periods.

Class 25, other crops. Rainfed crops, mainly summer grains, legumes or industrial crops. The fields may be grazed during fallow.

Class 26: River. Paraná River: deep running water which often carries sediments.

Appendix J

Class 1, intensively grazed grassland. All grassland classes with short grasses and less than 80% soil cover. Bright reflectance values in visible bands. It includes former classes 11, 12, 13, 14 and 16.

Class 2, not intensively grazed grassland. It is represented by tall close vegetation with different proportions of mixed leftover and green material. Normally, this class is geographically closely associated with burned areas. Class 2 includes former classes 1, 2, 5, 6 and 22.

Class 3, burned grassland. It is represented by burned and/or very short vegetation after fire, and burned remains. On these areas the image has low reflectance values in all bands. It includes former classes 7, 8, 9, and 10.

Class 4, erosion-bare soil. This class is represented by areas with almost no vegetation. In both images, it shows the highest brightness values in visible bands. It includes classes 17 and 18.

Class 5, forests. This class includes both, riparian and non riparian forest. Therefore, classes 3 and 4 are included here. This class has range use as will be discussed later.

Class 6, open forest. Like in the former 26-class classification it is represented entirely by class 15. This class has range use as will be discussed later.

Class 7, water. This class includes all those water resources which have no grass layer. It has therefore no range use other than watering. It includes former classes 21, 23 and 26.

Class 8, other. All classes (except water) which at the moment of the newest image (2005) had no range use. It includes former classes 19, 20, 24 and 25.

Curriculum vitae

Born, October 14, 1973 in Oberá, Misiones, Argentine

Nationality, Argentine

Family status, married

Education

1992/1998 - Studies of Agricultural Sciences at the National University of the North-East, Corrientes, Argentine. 1998 - Agricultural engineer degree

Current Position

Researcher. Department of Natural Resources, National Institute for Agricultural Technology (INTA), Corrientes, Argentine

Teacher assistant. National University of the North-East, Agricultural Sciences Faculty, Department of Water and Soil

Languages

Spanish - mother tongue

English - fluent in speaking, reading, writing

German - fluent in speaking, reading, poor in writing

Portuguese - fluent in speaking, reading, poor in writing

Professional Experience

At the Ministry of Production and Development, Corrientes, Argentine (1998 to 1999)

Memberships

Association for the Promotion of ARTS

Society of Agricultural Engineers, Corrientes, Argentina

Acknowledgements

This thesis would not have been possible without the support of many.

First of all, I would like to thank Him.

I would like to express my sincere gratitude and special thanks to Dr. Jürgen Schellberg and Dr. Matthias Braun for their valuable guidance.

I would like to thank DAAD for giving me the opportunity to study in Germany. In addition, my thanks to INTA Corrientes and Faculty of Agriculture-UNNE for giving me the authorization and support to study in Germany.

I am also thankful to Prof. Dr. Marc Janssens for accepting to be the chairman of my thesis defence.

My special thanks to the ARTS coordinators, Ms. Susanne Hermes and Mr. Jürgen Simons for their friendship and constant help.

My thanks also go to all ZFL members for their help and friendship. Especially to Mr. Jonas Franke for his helpful suggestions that improved this work.

I would also like to thank Mr. Attila Lüttmerding for his helpful suggestions and comments that improved this work.

My thanks also go to all INTA Corrientes staff. Especially thanks to the staff of Natural Resources, and Forages department for their support during the field campaign. Especially thanks to Mr. Daniel Ligier and to Ms. Cristina Goldfarb.

Thanks to Mr. Roberto Quinonez, Rosa Lencinas, Humberto Matteo, Osvaldo Vallejos, Ruth Perucca, Francisco Nuñez, Oscar Quiros, Raul Aranda, Juan Aranda and Antonio Prieto.

Thanks to all my friends in the ARTS program. And thanks to my friends in Bonn and Köln.

Last but not least, my deepest thank to my lovely wife for her constant love support and encouragement. Similarly, thanks to our families for their prayers and encouragement.